Effects of arketamine on reduced bone mineral density in mice: A role of gut microbiota

(マウスにおける骨密度低下におけるアールケタミンの効果：腸内細菌の役割)

2024 年 4 月提出

千葉大学大学院医学薬学府

先端医学薬学専攻

（主任：五十嵐　禎人 教授）

万 夏云

CONTENTS

1. Introduction

Osteoporosis, the common bone disease, is characterized by low bone mass and structural deterioration of bone tissue, leading to fragility of the bone. It is well known that people with osteoporosis have depression, suggesting depression as a risk factor for osteoporosis (Cizza et al., 2009; Wu et al., 2009). Furthermore, bone mineral density (BMD) in patients with depression is lower than that of subjects without depression (Schweiger et al., 2016; Yirmiya et al., 2009), suggesting depression as a risk factor for low BMD. Meta-analyses demonstrated that depression is a risk factor for low BMD, especially in women (Cizza et al., 2010; Schweiger et al., 2016; Wu et al., 2009; Yirmiya and Bab, 2009). While antidepressants, including selective serotonin reuptake inhibitors (SSRIs) and serotonin noradrenaline reuptake inhibitors (SNRIs), are widely used to treat depression, antidepressant use is associated with fractures in elderly people with osteoporosis (Agarwal et al., 2020; Kindilien et al., 2018; Rizzoli et al., 2012; Wadhwa et al., 2017). Therefore, it is important to develop the novel drugs which can produce antidepressant effects for depression in patients with osteoporosis.

Multiple lines of evidence indicate that the *N*-methyl-D-aspartate receptor antagonist (*R,S*)-ketamine can exert rapid and sustained antidepressant effects in patients with severe depression. Although (*S*)-ketamine (esketamine) nasal spray has been approved for treatment-resistant depression in the United States and Europe, we propose that another enantiomer, (*R*)-ketamine (arketamine), could serve as a novel rapid-acting antidepressant that does not cause the side effects associated with (*R,S*)-ketamine and esketamine (Hashimoto, 2019; 2020; 2022; Wei et al., 2022a). Moreover, a single dose of arketamine significantly improved the plasma levels of RANKL (receptor activator of nuclear kappa-B ligand) and ratio of osteoprotegerin to RANKL in susceptible mice after chronic social defeat stress (CSDS) (Xiong et al., 2019; Zhang et al., 2018). Additionally, arketamine remarkably alleviated the decreases in cortical and total BMD in the CSDS susceptible mice (Xiong et al., 2019) and ovariectomized (OVX) mice (Fujita and Hashimoto, 2020). Overall, arketamine is a promising drug for the treatment of both reduced BMD and depression in MDD patients (Wei et al., 2022a). However, the precise mechanisms underlying the beneficial effects of arketamine on BMD reduction remain elusive.

A growing body of evidence indicates that the gut microbiota has a critical role in health and disease states, particularly osteoporosis (Chang et al., 2022; Fan et al., 2021; Seely et al., 2021; Wei et al., 2022b; Zhang et al., 2021). Intriguingly, the gut microbiome is believed to possibly play an essential role in the remodeling of bones and maintenance of bone health, by regulating the immune system (Hernandez et al., 2022; Lu et al., 2021; Tu et al., 2021; Zhong et al., 2021).

The present study was undertaken to investigate whether gut microbiota play a role in the beneficial effects of arketamine in OVX model and CSDS model. First, we examined the effects of arketamine on reduced BMD of OVX mice and CSDS susceptible mice. Second, we performed 16S rRNA gene amplicon sequencing of feces samples for gut microbiota analysis. Third, an auxiliary non-targeted metabolomic analysis of plasma samples was performed because the gut microbiota plays a role in the generation of certain metabolites (Chang et al., 2022; Krautkramer et al., 2021; Lavelle and Sokol, 2020; Rooks and Garrett, 2016).

2. Materials and Methods

2.1. Animals

We performed this study using male/ female C57BL/6 mice aged 8 weeks (weight = 20–25 g; Japan SLC,

Inc., Hamamatsu, Japan) and male CD1 mice aged 13–15 weeks (weight > 40 g; Japan SLC, Inc). All animals were maintained at a constant room temperature of 23°C and relative humidity of 55 ± 5%, with a 12-hour light/dark cycle (illuminated between 7:00 and 19:00) and free access to food and water. We obtained approval for the study protocol from the Institutional Animal Care and Use Committee of Chiba University (permit number 2–389 and 4-377). Prior to sacrifice by cervical dislocation, deep anesthesia with isoflurane was administered to all animals. We did our best to minimize the suffering of animals.

2.2. Materials

Arketamine hydrochloride was prepared through the recrystallization of (*R,S*)-ketamine (ketamine hydrochloride; Ketalar®; Daiichi Sankyo Pharmaceutical Co., Ltd., Tokyo, Japan) and D-(-)-tartaric acid, as previously reported (Zhang et al., 2014). The dose of arketamine (10 mg/kg; hydrochloride dissolved in saline) used in previous reports was also applied herein (Qu et al., 2017). All other agents used were purchased commercially.

2.3. CSDS model, treatment, and sample collection

We induced CSDS according to our previous reports (Xiong et al., 2019). The C57BL/6 mice were exposed to aggressive CD1 mice for 10 min per day for 10 days. Following social defeat training, resident CD1 mice and intruder mice were divided by inserting porous Plexiglas separators into the cages for the remainder of the 24-hour experimental period. All animals were housed individually 24 hours after the final treatment. A social interaction test was carried out on day 11 to distinguish subpopulations of mice susceptible and not susceptible to social defeat stress. The mice were positioned inside an interactive testing box (42 × 42 cm) with an empty metallic mesh cage (10 × 4.5 cm) at one end. The motility of the mice was tracked over a 2.5-minute period, including in the presence of an unacquainted aggressor restricted to the metallic mesh cage for 2.5 min. Using a stopwatch, the time spent in the "interaction zone" (a 8-cm-wide area around the metallic mesh cage) was recorded. The interaction ratio was calculated as follows: time spent in the interaction area with the aggressor/time spent in the interaction area without the aggressor. An interaction ratio of 1 was the threshold value: mice scoring < 1 were classified as “susceptible” to social defeat stress and mice scoring ≥ 1 were considered “resilient”. Approximately 70%–80% of the mice were classified as susceptible following CSDS, and were randomized to conditions in the subsequent experiments. No-CSDS (control) C57BL/6 mice were caged prior to behavioral testing.

The CSDS susceptible mice were assigned to groups administered saline (10 ml/kg, intraperitoneal [i.p.]) or arketamine (10 mg/kg, i.p.) on day 12 (**Figure 1A**). The sucrose preference test (SPT) was conducted on day 14 to assess the effects of arketamine on the anhedonia-like phenotype (**Figure 1A**).

On the morning of day 15, fresh fecal samples were collected into microtubes containing liquid nitrogen and stored at −80°C within 1 hour until DNA extraction for 16S rRNA gene sequencing. On the morning of day 15, mice were anesthetized (inhalation of 5% and 3% isoflurane for induction and maintenance, respectively), and plasma samples were obtained and preserved at −80°C until untargeted metabolomics analysis. Subsequently, mouse brains were dissected, and femurs were harvested and fixed in 4% paraformaldehyde overnight at 4°C. The samples were then washed with phosphate-buffered saline, dehydrated in a graded ethanol series (25%, 50%, 75%, and 100%), and stored in 100% ethanol at 4°C until BMD measurements, as previously reported (Fujita and Hashimoto, 2020).

2.4. Ovariectomy, treatment, and sample collection

A total of 27 female mice were randomly and equally divided into three groups. All female mice used in the experiments were under isoflurane-induced anesthesia and underwent ovariectomy or sham surgery on day 0. After the mice were anesthetized, hair on the back below the rib was shaved, betadine was used to sterilize the surgical area, and a 1-2 cm incision was made in the skin and muscle layer under the rib on one side to locate the ovary, ligate the fallopian tube and remove the ovary. The muscle layer and skin were then sutured and disinfected. The same procedure was performed on the opposite side. Mice in the sham-operated group underwent the same procedure, except for ovaries removal and tubal ligation. Subsequently, arketamine (10 mg/kg/day, twice weekly) or saline (10 ml/kg/day, twice weekly) was administered intraperitoneally (i.p.) to mice for 6 weeks (day 1–day 39). On the morning of day 43, fresh fecal samples were collected from all mice for 16S ribosomal RNA sequencing and short-chain fatty acids (SCFAs) assay. On the afternoon of day 43, femur samples were collected and maintained in 4% paraformaldehyde, 4°C overnight, for subsequent bone mineral density (BMD) measurements. Furthermore, plasma samples were collected and stored at -80℃ for untargeted metabolomics analysis. On the morning of day 44, femurs were washed with phosphate saline buffer, merged with 25%, 50%, 75%, and 100% ethanol, and stored at 4°C until measurement of BMD as previously reported (Fujita and Hashimoto, 2020).

2.5. SPT

Mice were exposed to water and a palatable sucrose solution (1%) for 48 hours, deprived of food and water for 4 hours, and then exposed to two identical bottles for 1 hour (one containing the 1% sucrose solution and the other containing water). Sucrose and water intake were determined at the end of the test by weighing the pre-weighed bottles containing sucrose solution and water. The sucrose preference was given by the ratio between the amount of sucrose solution consumed and total liquid consumed.

2.6. Measurement of bone mineral density (BMD)

CT imaging system (LaTheta LCT-200; Hitachi Arouca Medical, Tokyo, Japan) was employed to determine the density of cortical, cancellous, planar, and total bone of the femoral neck. The LaTheta software (version 3.40) was used to measure and quantify the bone mineral density as previously reported (Fujita and Hashimoto, 2020; Xiong et al. 2019).

2.7. 16S rRNA sequencing analysis and measurement of SCFAs

Total DNA was obtained from mouse fecal samples and amplification of the V3–V4 hypervariable region of the 16S rRNA gene was performed by polymerase chain reaction (PCR) using universal bacterial primers. The purified PCR products were then sequenced at MyMetagenome Co, Ltd. (Tokyo, Japan) or BGI JAPAN K.K. (Kobe, Japan). These data are preserved in the National Center for Biotechnology Information sequence reads archive (PRJNA768302 and PRJNA912388).

Based on species profiles, we calculated within-sample (α) diversity to estimate the richness and evenness of the gut microbiota according to the observed species, Observed otus, ACE, etc.. For β-diversity analysis, the UniFrac distance metric was used to assess the structural variation of microbial communities across samples, and the results were visualized by principal coordinate analysis (PCoA). Linear discriminant analysis (LDA) was used to detect biomarkers in distinct sample groups, and the linear discriminant analysis effect size (LEfSe) was calculated for each biomarker (Segata et al., 2011).

The PICRUSt2 pipeline (Douglas et al., 2020) and operational taxonomic unit counts were used to

predict metagenome functions, and the MetaCyc metabolic pathway database was used for pathway abundance predictions. Welch's t-test was applied using STAMP (Parks et al., 2014) to compare the predicted abundance of MetaCyc pathways between groups.

2.8. Non-targeted metabolomics profiling of plasma samples

Analysis was performed on an ExionLC AD UPLC system (SCIEX, Tokyo, Japan) interfaced with an X500R LC-QToFMS system (SCIEX, Tokyo, Japan) with electrospray ionization (ESI) operated in both positive and negative ion modes. After adding the 100 μL methanol containing internal standards (100 nM *N*,*N*-diethyl-2-phenylacetamide, and d-camphor-10-sulfonic acid), plasma samples (100 μL) were centrifuged at 14000 × rpm for 5 minutes. After centrifuge, the supernatant was transferred to Amicon® Ultra-0.5 3 kDa filter columns (Merck Millipore, Tokyo, Japan) and centrifuged at 14000 × rpm for 1 hour. Filtrates were transferred to glass vial for analysis.

The metabolome data was analyzed by Mass Spectrometry - Data Independent AnaLysis (MS-DIAL) software version 4.60 (https://www.nature.com/articles/nmeth.3393) and R statistical environment Ver 4.0.5 (Tsugawa et al., 2014). In this study, metabolomes were detected at least 50% from the analyzed samples, and the coefficient of variation (CV) values of 30% of metabolomes, and annotation level 2 proposed by Schymanski et al. (Schymanski et al., 2014) (https://pubs.acs.org/doi/10.1021/es5002105) were used for data analysis. Peak heights were nomadized by peak heights of internal standards and locally weighted least-square regression (locally estimated smoothing function, LOESS) and cubic spline with QC samples.

Metabolomics data were subjected to orthogonal partial least square discriminant analysis (OPLS-DA) with SIMCA 14.0 software (Sartorius AG, Göttingen, Germany), which was also used for the construction of multivariate statistical models. Significant peaks were determined by combination of variable importance in projection (VIP) value > 0.3 (OVX model) or 0.4 (CSDS model), and Wilcox rank test P values < 0.05 (FDR < 0.51 [OVX model] or FDR < 0.23 [CSDS model]).

2.9. Statistical analysis

Comparisons between two groups were performed with the Wilcox test, comparisons between three groups were performed using ANOVA or Kruskal-Wallis test, followed by Tukey or Fisher's least significant difference post hoc test, according to the data distribution. Repeated-measures data were statistically analyzed using repeated-measures analysis of variance (ANOVA). For β-diversity analysis, differences between the groups were analyzed using analysis of similarities (ANOSIM). The P-values of less than 0.05 were considered statistically significant. The FDR was calculated to control for multiple comparisons, as appropriate. P-values ≤ 0.05 were considered statistically significant.

3. Results

3.1. Part 1 (CSDS model)

3.1.1. Effects of arketamine on the anhedonia-like phenotype and reduced BMD in CSDS-susceptible mice

To check for anhedonia-like behavior in CSDS susceptible mice, we performed the SPT, a classical test of anhedonia-like behavior in rodents. The SPT data showed that sucrose preference was significantly reduced

in CSDS susceptible mice compared with control mice. The reduction in sucrose preference was reversed after a single dose of arketamine (10 mg/kg) (**Figure 1B**), consistent with our previous report (Xiong et al., 2019).

Next, we compared BMD among the control, CSDS + saline, and CSDS + arketamine groups using representative computed tomography images of the femurs in each group (**Figure 1C**). Compared with the control group, mice in the CSDS + saline group had significantly decreased cortical and total BMD (**Figure 1D**). A single dose of arketamine (10 mg/kg) significantly improved these reductions of BMD in CSDS susceptible mice (**Figure 1D**). In contrast, cancellous and planar BMD were not different among the three groups (**Figure 1D**), consistent with our previous report (Xiong et al., 2019). Next, we performed Pearson correlation analysis to further explore the potential relationship between BMD and anhedonia-like behavior in mice. Positive correlations were found between sucrose preference and cortical BMD (and total BMD) in all three groups (**Figure 1E**).

These data show that a single dose of arketamine can improve the anhedonia-like phenotype and reduce cortical (and total) BMD in CSDS susceptible mice.

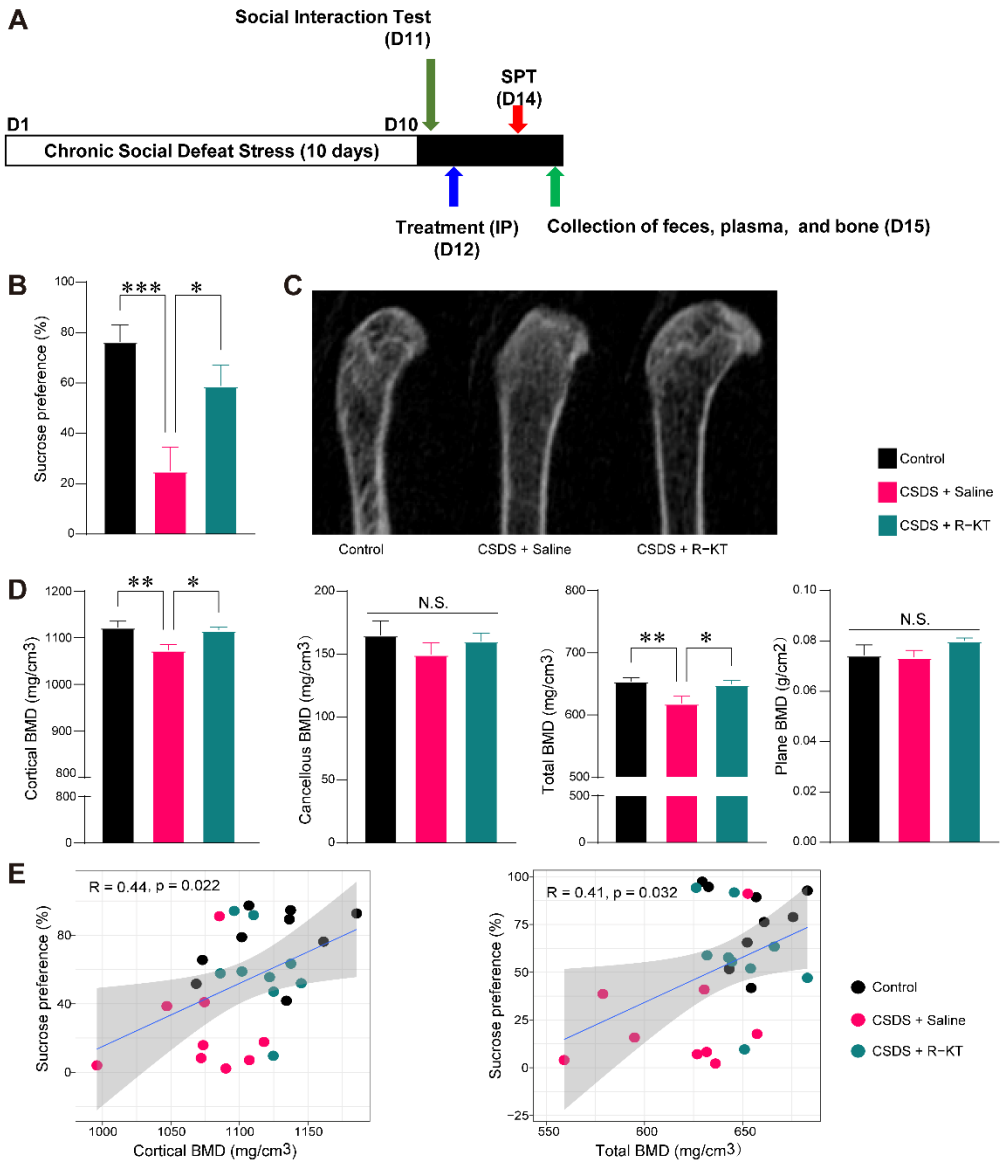

Figure 1. Illustration of the experimental schedule and the effect of arketamine on anhedonia-like behavior and reduced BMD in CSDS susceptible mice

A: Experimental schedule. CSDS (chronic social defeat stress) was conducted from days 1 to 10, followed by a social

interaction test (SIT) on day 11. On day 12, CSDS susceptible mice were administered with saline (10 ml/kg, i.p.) or arketamine (10 mg/kg, i.p.). Control (no CSDS) mice received saline (10 ml/kg, i.p.). The SPT was performed on day 14. Feces, plasma, and femur samples were collected from all mice on day 15. B: Sucrose preference of SPT (Kruskal-Wallis test, $P = 0.0023$). C: Representative microcomputed tomography (CT) scans and images showing the femur mass in the three groups. D: Arketamine improved reduction of femoral BMD in the CSDS susceptible mice (cortical BMD: one-way ANOVA, $F_{(2, 24)} = 6.08$, $P = 0.007$; total BMD: one-way ANOVA, $F_{(2, 24)} = 5.79$, $P = 0.009$; cancellous BMD: one-way ANOVA, $F_{(2, 24)} = 0.72$, $P = 0.49$; plane BMD: one-way ANOVA, $F_{(2, 24)} = 1.49$, $P = 0.25$). E: Pearson correlation analysis of sucrose preference of SPT and cortical BMD or total BMD in the three groups. The values represent the mean ± S.E.M. ($n = 9$). *$P < 0.05$, **$P < 0.01$, ***$P < 0.001$, N.S.: not significant. SPT: 1% sucrose preference test.

3.1.2. Composition of the gut microbiota

To explore alterations in the gut microbiota profile of CSDS susceptible mice, and the effects of arketamine on the gut microbiota, we carried out 16S rRNA sequencing of fecal contents from all three groups. Regarding α-diversity, the observed species richness was significantly higher in the CSDS + saline group than control group, whereas the Chao 1, ACE, and Shannon indices were not different among the three groups (**Figure 2A**). Regarding β-diversity, weighted UniFrac analysis of PCoA plots revealed distinct microbiome clusters (**Figure 2B**). According to the weighted UniFrac distances, there were significant differences in gut microbiome composition in the CSDS + saline and CSDS + arketamine groups compared with the control group (**Figure 2B**).

Taxonomic composition analysis revealed 9 identified phyla and 129 identified species (**Figure 2C**). *Firmicutes* represented the predominant phylum (relative abundance = 74.5% in the control group, 53.9% in the CSDS + saline group, and 50.8% in the CSDS + arketamine group), followed by *Bacteroidetes* (relative abundance = 23.1% in the control group, 43.6% in the CSDS + saline group, and 45.9% in the CSDS + arketamine group) (**Figure 2C**). At the species level, the most dominant species was *Lactobacillus animalis* (10.8% in the control group, 15.1% in the CSDS + saline group, and 12.9% in the CSDS + arketamine group), followed by *Barnesiella intestinihominis* (6.6% in the control group, 10.6% in the CSDS + saline group, and 11.6% in the CSDS + arketamine group) (**Figure 2C**).

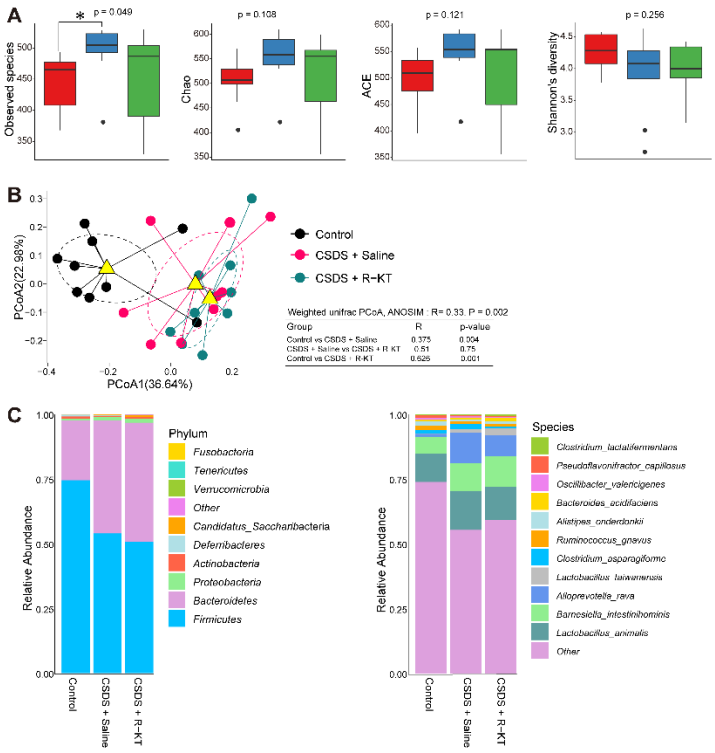

Figure 2. Alpha-diversity, beta-diversity and composition of gut microbiota

A: Alpha-diversity of gut microbiota in the three groups. Observed species index Kruskal-Wallis test, P = 0.049, Chao index Kruskal-Wallis test, P = 0.108, Ace index Kruskal-Wallis test, P = 0.121, Shannon's diversity Kruskal-Wallis test, P = 0.256. B: Beta-diversity of gut microbiota in the three groups. C: Bar charts of bacterial community composition at the phylum level and species level, with the species level showing the 11 most abundant bacteria across all samples and the rest shown as "other". The box shows the interquartile range of 25 to interquartile 75, the line shows the median and whiskers show the minimum and maximum values. The number of each group (n = 9). *P < 0.05.

3.1.3. Taxonomic signatures of the gut microbiota

To detect specific bacteria associated with each group, LDA was used to identify taxonomic biomarkers (LEfSe > 3.9). The family *Prevotellaceae*, genus *Alloprevotella*, and species *Alloprevotella rava* were associated with the CSDS + saline group (**Figure 3A, 3B**). LDA also identified seven biomarkers for the CSDS + arketamine group, including the phylum *Bacteroidetes*, order *Bacteroidales*, class *Bacteroidia*, genus *Barnesiella,* and three species (*Barnesiella intestinihominis*, *Lactobacillus taiwanensis*, and *Streptococcus danieliae*) (**Figure 3A, 3B**).

Next, we focused on taxonomic features that were significantly different between the CSDS + saline and control groups, as well between the CSDS + arketamine and CSDS + saline groups. At the phylum level, increased *Bacteroidetes*, *Candidatus Saccharibacteria*, *Proteobacteria*, and decreased *Firmicutes* were seen in the CSDS + saline group. *Deferribacteres* were reduced in the CSDS + arketamine group compared with the CSDS + saline group (**Figure 3C**).

In the CSDS + saline group, increases were seen in *Alistipes finegoldii*, *Alloprevotella rava*, *Bacteroides massiliensis*, *Clostridium scindens*, *Lactobacillus taiwanensis*, *Streptococcus danieliae*, and *TM7 phylum*, while there were decreases in *Acetanaerobacterium elongatum*, *Acetatifactor muris*, *Anaerotruncus colihominis*, *Blautia faecis*, *Clostridium aldenense*, *Clostridium leptum*, *Clostridium methylpentosum*, *Eubacterium coprostanoligenes*, *Eubacterium eligens*, *Flavonifractor plautii*, *Intestinimonas*

butyriciproducens, *Oscillibacter valericigenes*, *Parvibacter caecicola*, *Pseudoflavonifractor capillosus*, and *Ruminococcus gnavus* (**Figure 3D**). Compared with the CSDS + saline group, the abundances of *Acetanaerobacterium elongatum*, *Blautia faecis*, and *Mucispirillum schaedleri* were lower in the CSDS + arketamine group, while that of *Parabacteroides merdae* was significantly higher (**Figure 3D**).

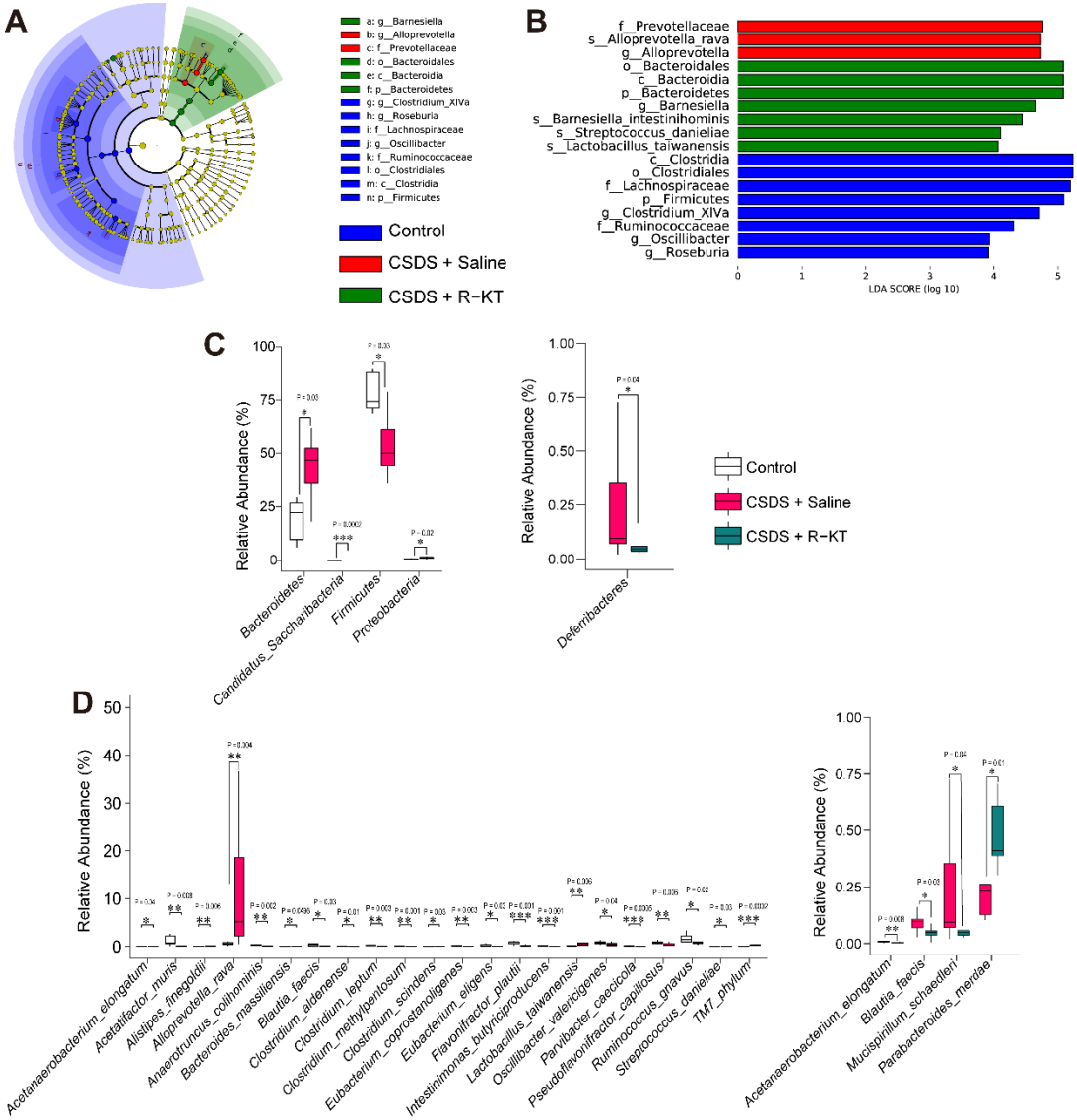

Figure 3. Analysis of gut microbial biomarkers using LEfSe, differential taxonomic microbes between the groups
A: Taxonomic cladogram derived from LEfSe analysis. B: Taxa were selected as $P < 0.05$ and linear discriminant analysis (LDA) scores > 3.9. C: Differences in the relative abundance of gut microbiota between the two groups at the phylum level (Wilcox test). D: Differences in the relative abundance of gut microbiota between the two groups at the species level (Wilcox test). The box shows the interquartile range of 25 to interquartile 75, the line shows the median and whiskers show the minimum and maximum values. The number of each group ($n = 9$). *$P < 0.05$, **$P < 0.01$, ***$P < 0.001$.

3.1.4. Functional annotation of the 16S rRNA gene

PICRUSt2 analysis was performed to predict the metagenomic functional components of the gut microbiota. The resulting functional profiles emphasized that 36 pathways (Welch's t-test, $q < 0.05$) were significantly altered in the CSDS + saline group compared with the control group. The types of microbial functions

dysregulated in the CSDS + saline group included adenosylcobalamin metabolism, tetrahydrofolate metabolism, the tricarboxylic acid (TCA) cycle, pyruvate metabolism, and L-arginine metabolism. (**Figure 4**). Furthermore, 13 metabolic pathways (Welch's t-test, $p < 0.05$) were significantly altered in the CSDS + arketamine group compared with the CSDS + saline group, including catechol metabolism, glucose metabolism, and aromatic compounds metabolism. Of note, arketamine significantly improved the elevated activity of both the TCA cycle I (prokaryotic) and TCA cycle VI (obligate autotrophs) pathways in CSDS-susceptible mice (**Figure 4**).

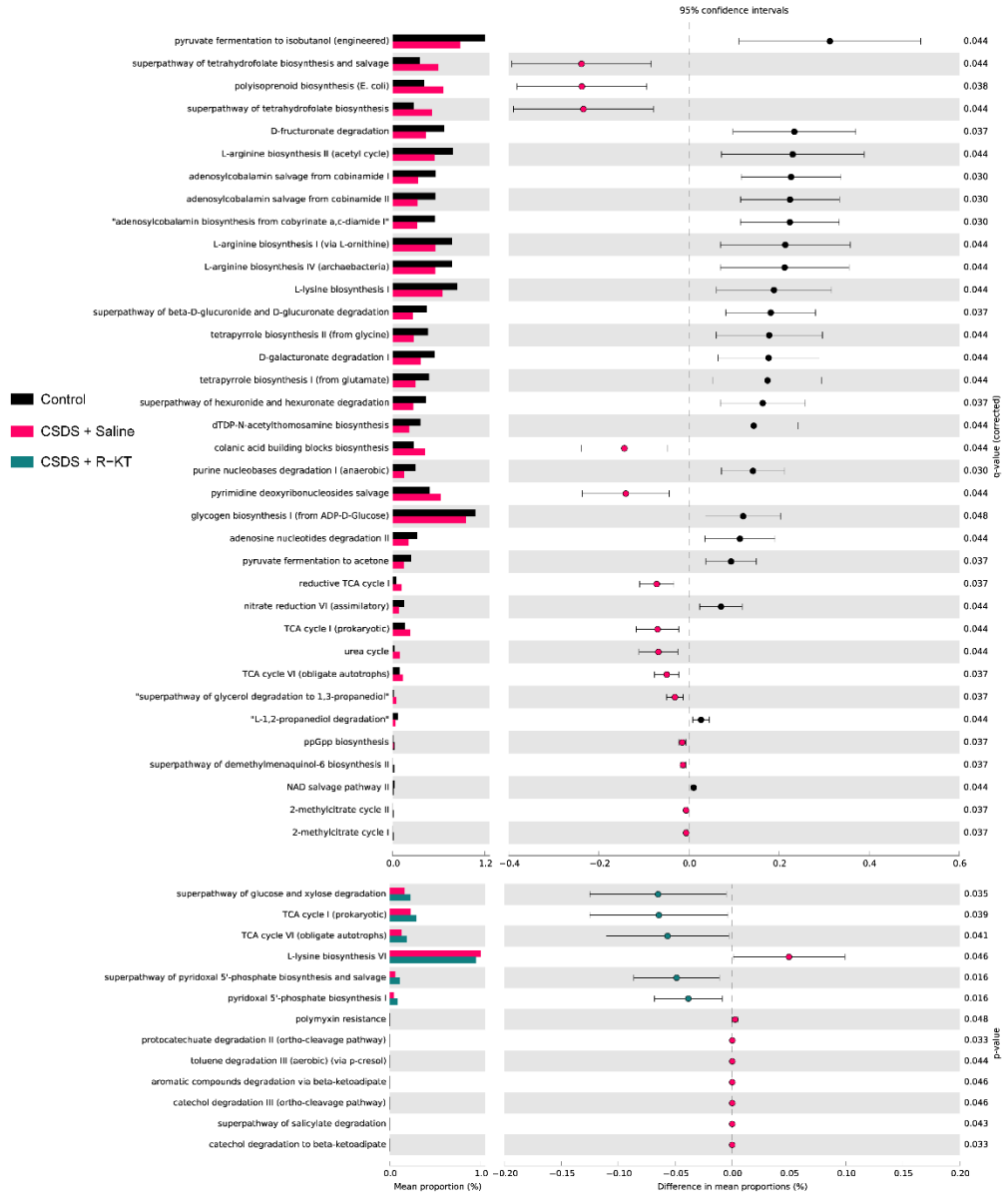

Figure 4. Comparison of differential functions in MetaCyc database predictions with PICRUSt2 using 16S data
Significant alterations in the MetaCyc metabolic pathway between the two groups that are predicted based on sequencing data of the 16S rRNA gene.

3.1.5. Metabolomic analysis of plasma samples

We also investigated the plasma metabolome of the three groups. A total of 91 metabolites were detected with high confidence using a comprehensive metabolite analysis protocol. OPLS-DA score plots revealed separation between the CSDS + saline and control groups, as well as between the CSDS + saline and CSDS + arketamine groups (**Figure 5A**).

Volcano plots were constructed based on p-values from the Wilcox test and VIP scores from the OPLS-

DA model, derived through comparison of the control and CSDS + saline groups (**Figure 5B**) and CSDS + saline and CSDS + arketamine groups (**Figure 5D**). Six metabolites, including 9-(5-o-methylpentofuranosyl)-1,9-dihydro-6H-purin-6-one, N-(1H-indol-5-yl)benzamide, D-mannitol, gamma-glutamate-glutamine, L-arginine, and vitamin C, exhibited significantly higher expression in the CSDS + saline than control group (**Figure 5B, 5C**). Furthermore, six metabolites were differentially expressed between the CSDS + saline and CSDS + arketamine groups (**Figure 5D, 5E**). Interestingly, the plasma level of L-cystine in the CSDS + arketamine group was significantly higher than that in the CSDS + saline group (**Figure 5E**). The remaining five metabolites, 3-benzyl-5-methyl-1,2-oxazole-4-carboxylic acid, 5-bromo-1-benzofuran-2-carboxylic acid, 5-bromo-3-chloro-2-hydroxybenzoic acid, 9-(5-o-methylpentofuranosyl)-1,9-dihydro-6H-purin-6-one, and methyl 4-formyl-3-hydroxy-2-naphthoate, showed significantly lower expression in the CSDS + arketamine than in the CSDS + saline group (**Figure 5E**).

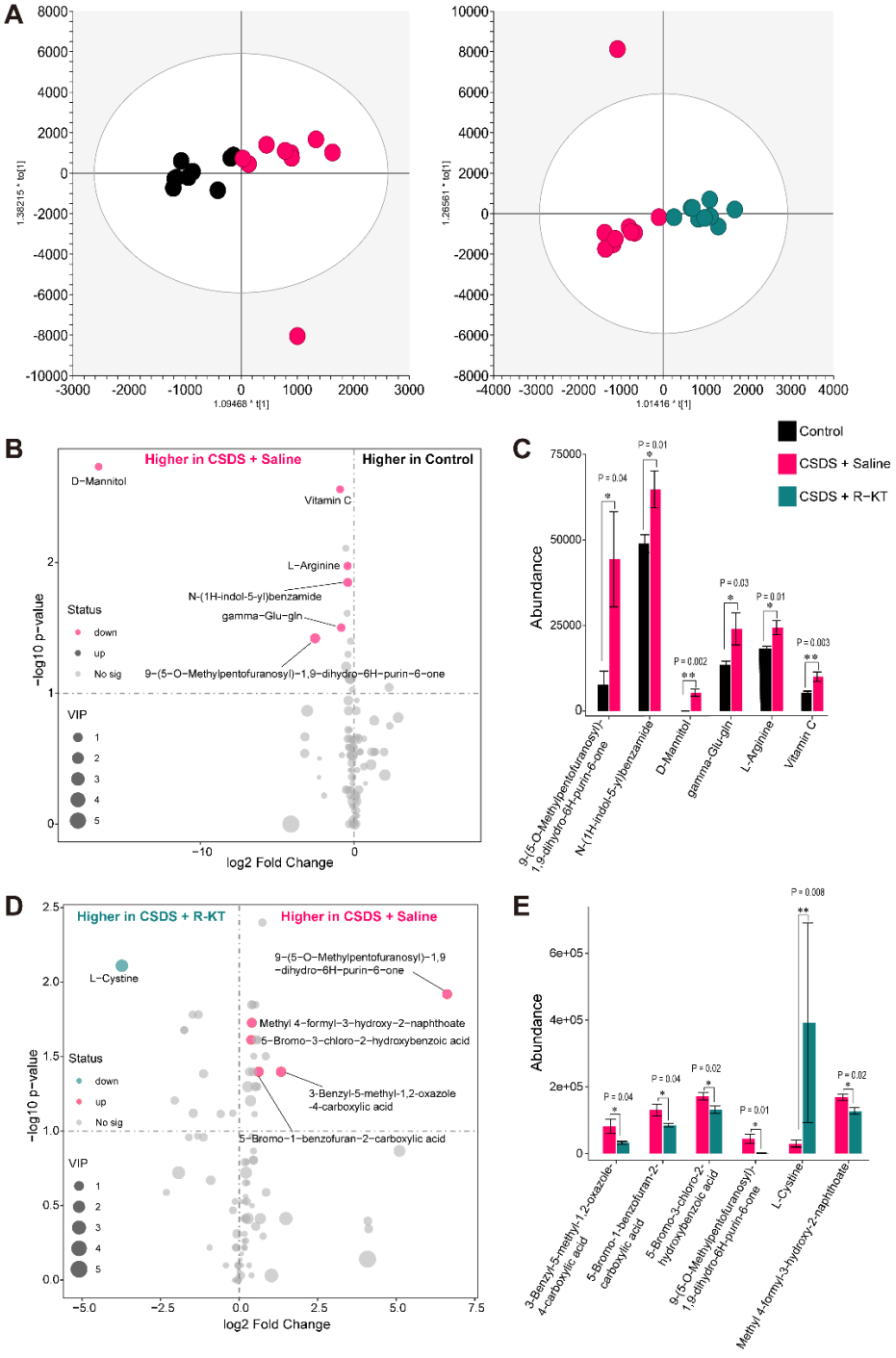

Figure 5. Metabolomic profiles of plasma samples

A: Scatter plot of plasma metabolites between the two groups based on OPLS-DA model. B and D: Volcano plots display plasma metabolite profiles between the two groups (B: control group and CSDS +saline group; D: CSDS + saline group and CSDS + arketamine group). X-axis represents log-transformed fold change in metabolite abundance, y-axis represents P-value for -log10 transformation by Wilcox test. Horizontal lines indicate $P < 0.05$. Colored dots indicate metabolites that differ between the two groups. C and E: Abundances of differential plasma metabolites between the two groups (C: control group and CSDS +saline group; E: CSDS +saline group and CSDS + arketamine group) (Wilcox test). Values represent the mean ± S.E.M. (n = 9). *P < 0.05, **P < 0.01.

3.1.6. Associations among anhedonia-like behavior, reduced BMD, dysregulated gut microbes, and metabolites

We further investigated whether there are associations among CSDS-induced anhedonia-like behavior, reduced BMD, dysregulated gut microbiota, and altered metabolites using Pearson correlation analysis. A heatmap demonstrated that the six metabolites elevated in the CSDS + saline group correlated with BMD and sucrose preference (**Figure 6A**). In particular, (5-o-methylpentofuranosyl)-1,9-dihydro-6H-purin-6-one, L-arginine, vitamin C, and gamma-glutamate-glutamine were significantly negatively correlated with cortical BMD, and the metabolite D-mannitol was negatively correlated with sucrose preference (**Figure 6A**).

Four microbes (*Clostridium methylpentosum*, *Pseudoflavonifractor capillosus*, *Intestinimonas butyriciproducens*, and *Acetatifactor muris*) with reduced abundance in the CSDS + saline group correlated strongly and positively with sucrose preference. The abundances of *Clostridium methylpentosum* and *Intestinimonas butyriciproducens* positively correlated with total BMD, while the abundances of microbes elevated in response to CSDS, namely, *Alistipes finegoldii* and *Alloprevotella rava,* negatively correlated with sucrose preference. Notably, the abundances of *Intestinimonas butyriciproducens*, *Eubacterium coprostanoligenes*, and *Parvibacter caecicola* were strongly and negatively correlated with the metabolite D-mannitol (**Figure 6B**).

Correlation network analysis demonstrated highly complex interactions among CSDS-induced anhedonia-like behavior, reduced BMD, dysregulated gut microbes, and metabolite alterations (109 correlations; Spearman rho ≥ 0.48, $p < 0.05$, FDR-corrected $p < 0.05$). The bacteria *Intestinimonas butyriciproducens*, the abundance of which was reduced in the CSDS + saline group, was significantly positively correlated with sucrose preference and significantly negatively correlated with the metabolite D-mannitol. In turn, D-mannitol was positively correlated with L-arginine and 9-(5-o-methylpentofuranosyl)-1,9-dihydro-6H-purin-6-one, while both L-arginine and 9-(5-o-methylpentofuranosyl)-1,9-dihydro-6H-purin-6-one were negatively correlated with cortical BMD (**Figure 6C**).

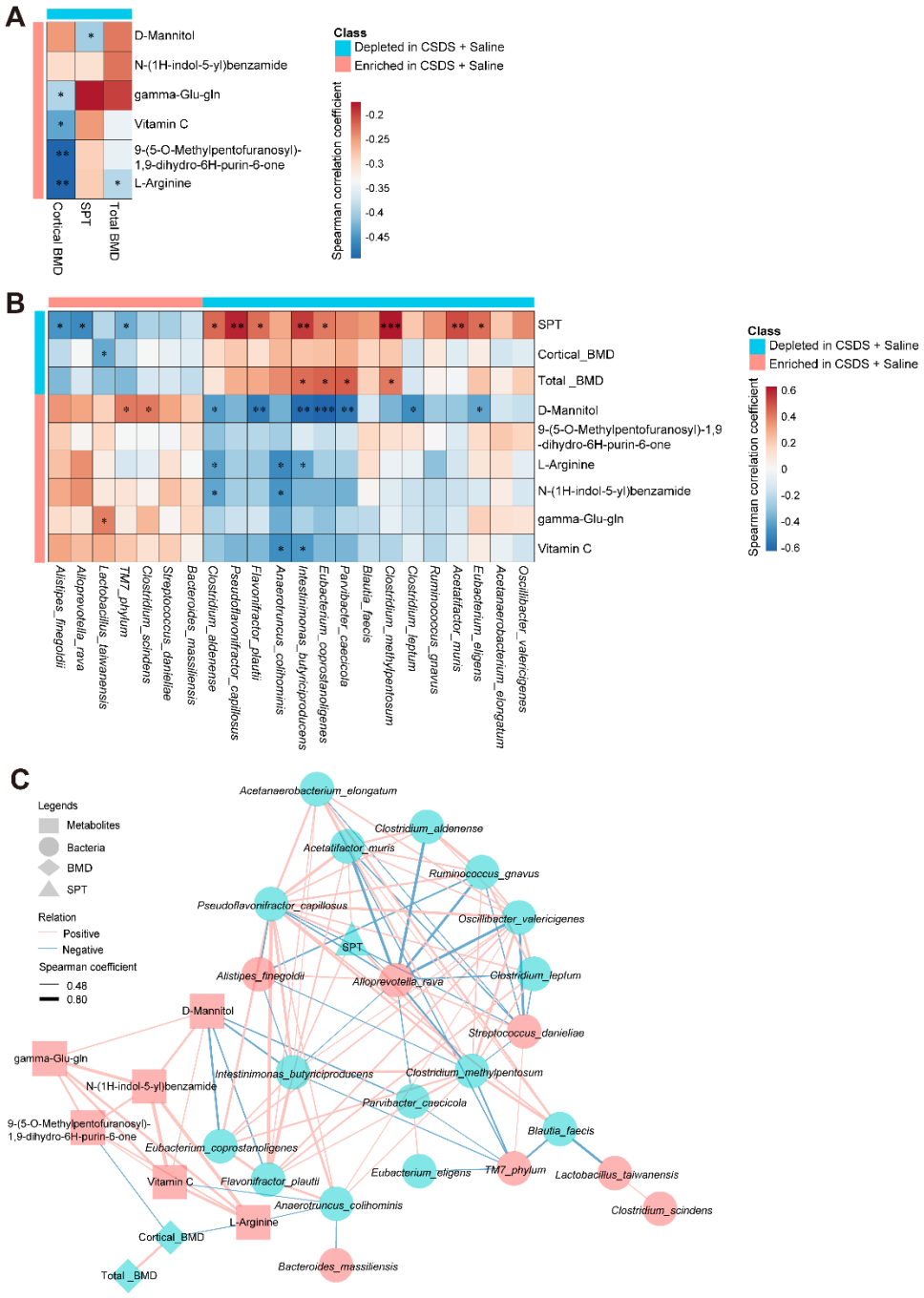

Figure 6. Correlation between anhedonia-like behavior, reduced BMD, dysregulated gut microbes, and metabolites

A: Spearman correlation analysis of plasma differential between control group and CSDS + saline group with total BMD, cortical BMD or SPT. B: Spearman correlation analysis of differential species (control group vs. CSDS + saline group) with differential metabolites (control group vs. CSDS + saline group), total BMD, cortical BMD or SPT. C: Network revealing the relationship between anhedonia-like behavior, reduced BMD, dysregulated gut mircrobes, and altered metabolites (Spearman's absolute correlation coefficient ≥ 0.48, FDR-corrected $P < 0.05$), with nodes representing enriched (red) or depleted (blue) features in the CSDS + saline group compared to the control group. The red line connecting the nodes indicates positive correlations and the blue line indicates negative correlations.

3.1.7. Associations among arketamine-induced phenotype improvements (anhedonia-like behavior, reduced BMD, gut microbial dysbiosis, and altered metabolites) in CSDS susceptible mice

Spearman's correlation analysis revealed a significant negative correlation between cortical BMD and an arketamine-induced reduction in the expression of the metabolite 9-(5-o-methylpentofuranosyl)-1,9-dihydro-

6H-purin-6-one (**Figure 7A**). The arketamine-induced reduction in the expression of the metabolite 3-benzyl-5-methyl-1,2-oxazole-4-carboxylic acid was positively correlated with the abundance of *Mucispirillum schaedleri*, while the arketamine-induced reduction in the expression of the metabolite 5-bromo-3-chloro-2-hydroxybenzoic acid was negatively correlated with the abundance of *Parabacteroides merdae* (**Figure 7B**). Correlation network analysis revealed complicated interactions among arketamine-induced improved phenotypes (anhedonia-like behavior, reduced BMD, dysregulated gut microflora, and metabolites) in CSDS susceptible mice. Three microbes (*Mucispirillum schaedleri*, *Blautia faecis* and *Acetanaerobacterium elongatum*) exhibited reduced abundance in the CSDS + arketamine group, and were negatively correlated with the microbe *Parabacteroides merdae*, which was in turn indirectly correlated with 9-(5-o-methylpentofuranosyl)-1,9-dihydro-6H-purin-6-one. The metabolite 9-(5-o-methylpentofuranosyl)-1,9-dihydro-6H-purin-6-one was also negatively correlated with cortical BMD (**Figure 7C**).

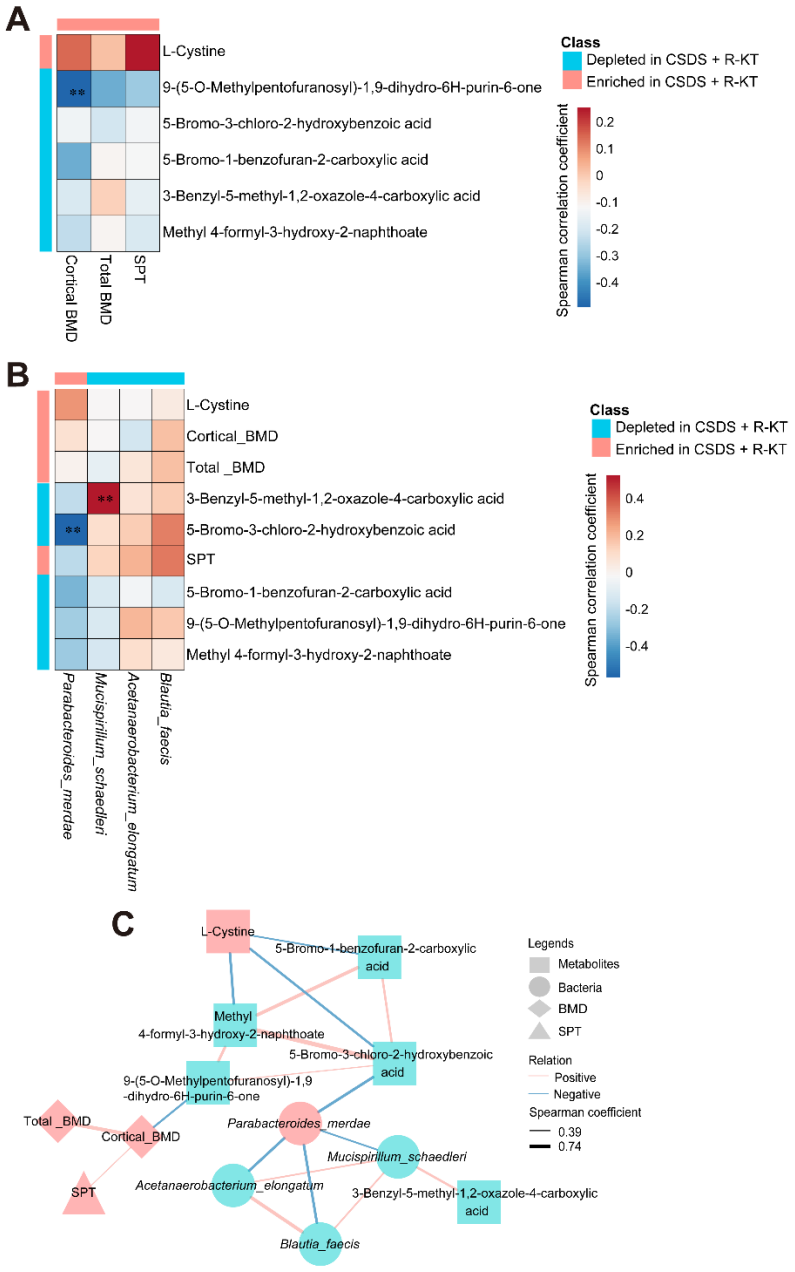

Figure 7. Correlation between arketamine-induced improved phenotypes (anhedonia-like behavior, reduced BMD, gut microbial dysbiosis, and metabolites) in CSDS susceptible mice

A: Spearman correlation analysis of plasma metabolites altered between CSDS + saline group and CSDS + arketamine groups, with total BMD, cortical BMD or SPT. B: Spearman correlation analysis of differential species (CSDS + saline group vs. CSDS + arketamine group) with differential metabolites (CSDS + saline group vs. CSDS + arketamine group), total BMD, cortical BMD or SPT. C: Network revealing the relationship between arketamine-induced improved phenotypes (anhedonia-like behavior, reduced BMD, gut microbial dysbiosis, and metabolites) in CSDS susceptible mice (Spearman's absolute correlation coefficient > 0.39, $P < 0.05$), with nodes representing enriched (red) or depleted (blue) features in the arketamine group compared to the CSDS + saline group. The red line connecting the nodes indicates positive correlations and the blue line indicates negative correlations.

3.2. Part 2 (OVX model)

3.2.1. Effects of arketamine on reduced BMD of OVX mice

Surgery of OVX or sham was performed on day 0. Subsequently, saline (10 ml/kg/day) or arketamine (10 mg/kg/day) was administered to mice from day 1 to day 39 (**Figure 8A**). Body weight of all mice was increased gradually. At the third, fourth, and sixth weeks after surgery, body weight of OVX + saline group and OVX + arketamine group was significantly higher than that in the sham + saline group (**Figure 8B**). Representative CT images of femurs from each group were shown (**Figure 8C**). Compared to the sham + saline group, cortical BMD and total BMD of OVX mice were significantly lower than those of sham + saline group (**Figure 8D and 8E**). Arketamine significantly ameliorated these reductions of OVX mice (**Figure 8D and 8E**). In contrast, there were no changes in cancellous BMD and plane BMD among the three groups (**Figure 8F and 8G**). The data are consistent with our previous report (Fujita and Hashimoto, 2020).

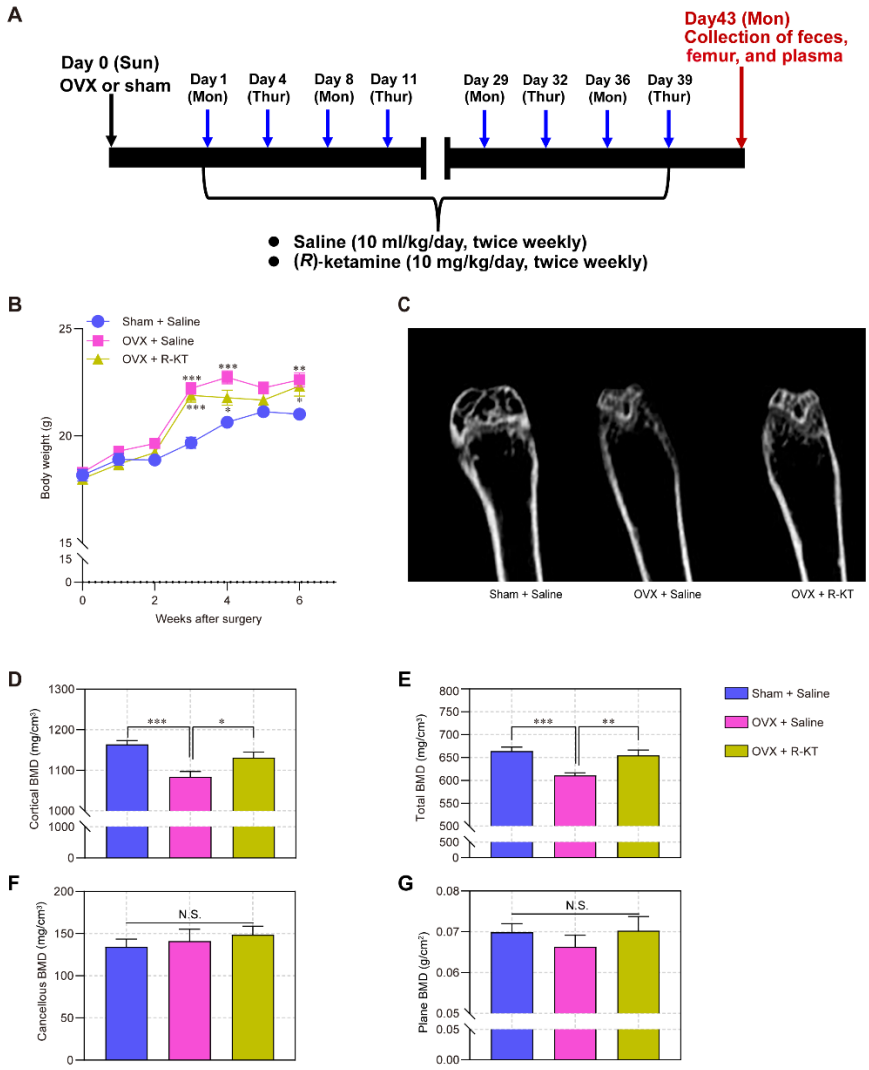

Figure 8. Experimental design and data of body weight change and BMD

A: Experimental schedule. Surgery for sham or ovariectomy (OVX) was performed on day 0 (Sunday). Subsequently, saline (10 ml/kg/day, twice weekly) or arketamine (10 mg/kg/day, twice weekly) was administered i.p. to mice for 6 weeks (day 1–day 39). In the morning of day 43, fresh fecal samples were collected from the mice. Then plasma samples were collected from all mice in the afternoon of day 43. B: Changes in body weight of three groups of mice. There were significant changes in body weight among the three groups (repeated-measures ANOVA, $F_{(7.14,\ 85.691)} = 13.919$, $P < 0.0005$). C: The representative image of femur bone mass observed by microcomputed tomography (CT). Arketamine

ameliorated the femur bone loss by OVX. D: Cortical BMD (one-way ANOVA, $F_{(2, 24)} = 11.07$, $P = 0.0004$). E: Total BMD (one-way ANOVA, $F_{(2, 24)} = 10.22$, $P = 0.0006$). F: Cancellous BMD (one-way ANOVA, $F_{(2, 24)} = 0.41$, $P = 0.67$). G: Plane BMD (one-way ANOVA, $F_{(2, 24)} = 0.58$, $P = 0.57$). The values represent the mean ± S.E.M. ($n = 9$). *$P < 0.05$, **$P < 0.01$, ***$P < 0.001$. BMD: bone mineral density. N.S.: not significant. OVX: ovariectomized. R-KT: arketamine.

3.2.2. Composition of gut microbiota

For α-diversity, observed _OTUs and ACE indices in OVX + arketamine were significantly greater than those in OVX + saline group although there were no changes in these indices between sham + saline group and OVX + saline group (**Figure 9A and 9B**). To determine the similarity (β-diversity) between microbial communities in each group, a principal component analysis (PCoA) was performed using the weighted UniFrac distance matrix. There were significant differences of β-diversity among the three groups (**Figure 9C**).

Next, we specified the relative proportions of dominant taxa at the phylum level. A total of 9 phyla were ultimately clarified in each group (**Figure 9D**). *Firmicutes* was the most dominant phylum with a relative abundance of 62.7% in the sham + saline group, 66.1% in the OVX + saline group, and 63.1% in the OVX + arketamine group. *Bacteroidetes* was second dominant phylum with a relative abundance of 35.1% in the sham + saline group, 31.3% in the OVX + saline group, and 34.3% in the OVX + arketamine group (**Figure 9D**).

We investigated the top 40 most abundant microbiome at the genus level (**Figure 9E**). The most dominant genus, *Lactobacillus*, was accounted for 41.1% across all samples. Based on the Bray-Curtis difference index, we clustered microbial community components to explore the microbial community profiles in each group. There was significant clustering between the sham + saline group and OVX + arketamine group. In contrast, there was no obvious clustering between the OVX + saline and sham + saline group or OVX + arketamine group (**Figure 9D and 9E**).

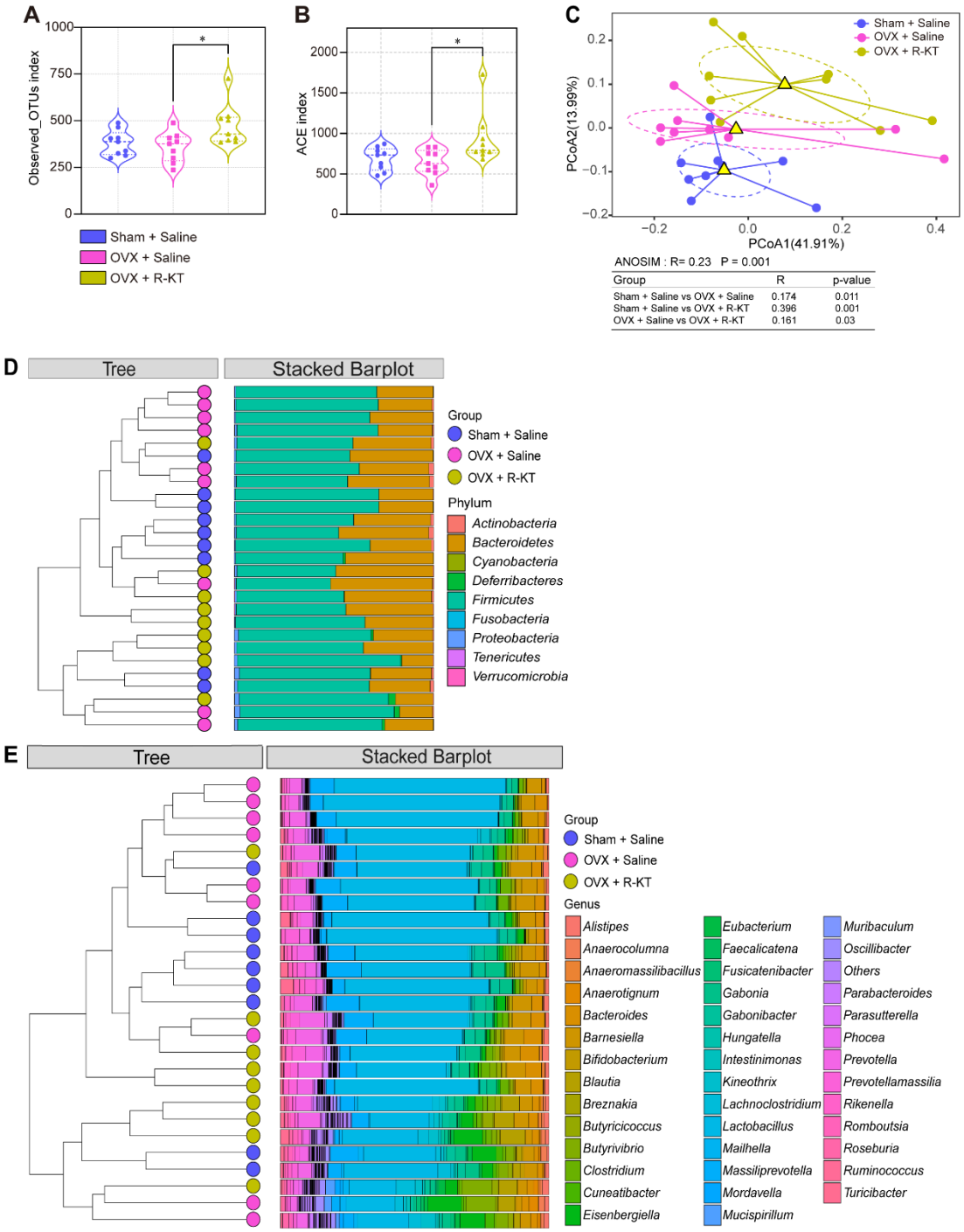

Figure 9. Alpha-diversity, beta-diversity and composition of gut microbiota

A: Observed_OTUs index (Kruskal-Wallis test, P = 0.035). B: ACE index (Kruskal-Wallis test, P = 0.037). C: Principal coordinate analysis based on weighted Unifrac distances (ANOSIM, R = 0.23, P = 0.001). D: Bacterial Composition at the phylum level. E: Bacterial Composition at the genus level. In violin plots, the horizontal dotted lines indicate median, quartiles. The number of mice in each group was n = 9. *P < 0.05. N.S.: not significant. OVX: ovariectomized. R-KT: arketamine.

3.2.3. Correlations of gut microbiota with BMD

Considering the role of gut microbiota in bone function, we hypothesized that altered gut microbiota abundances might be associated with beneficial effects of arketamine on reduced BMD in OVX mice. In this study, we pay attention to the gut microbiota that differed markedly in abundance between the OVX + saline and OVX + arketamine groups. The gut microbiota abundance in each group was then investigated at the

OTU and genus levels. Our results showed that 82 of 2838 OTUs and 6 of 188 genera reached statistically significant between OVX + saline group and OVX + arketamine group ($P < 0.05$, **Supplementary Table 1**). The distribution of the relative abundance of differential OTUs between the OVX + saline group and OVX + arketamine group was shown in **Supplementary Figure 1.** We quantified correlations between arketamine-related OTUs (or genera) and BMD using the Spearman correlation method (**Figure 10A and 10B**). We identified that the relative abundance of 9 OTUs, including OTU00061 (*Kineothrix*), OTU00077 (*Blautia*), OTU00220 (*Faecalicatena*), OTU00375 (*Magnetovibrio*), OTU00397 (*G_undefined_Ruminococcaceae*), OTU00453 (*Pseudoflavonifractor*), OTU00476 (*Flavonifractor*), OTU00600 (*Butyricicoccus*), and OTU00648 (*Faecalicatena*) were significantly negatively correlated with cortical BMD and total BMD or plane BMD. In contrast, the relative abundances of 16 OTUs such as OTU00012 (*Rikenella*), OTU00013 (*Turicibacter*), OTU00015 (*Gabonia*), OTU00021 (*Blautia*), OTU00042 (*Eisenbergiella*), OTU00113 (*Kineothrix*), OTU00129 *(Eubacterium*), OTU00161 (*Lachnoclostridium*), OTU00180 (*Alkaliphilus*), OTU00243 (*Eisenbergiella*), OTU00269 (*Anaeromassilibacillus*), OTU00286 (*Fusicatenibacter*), OTU00351 (Monoglobus), OTU00365 (Erysipelatoclostridium), OTU00547 (*Lachnoclostridium*), and OTU00778 (*Oscillibacter*) were significantly positively correlated with cortical BMD and total BMD or plane BMD (**Figure 10A**). At the genus level, *Turicibacter,* one of the arketamine-related genera, was positively correlated with cortical BMD (coefficient = 0.61, $P = 0.0007$) and total BMD (coefficient = 0.51, $P = 0.007$) (**Figure 10B**). These data suggest that the genera *Turicibacter* may play a role in the beneficial effects of arketamine in reduced BMD of OVX mice.

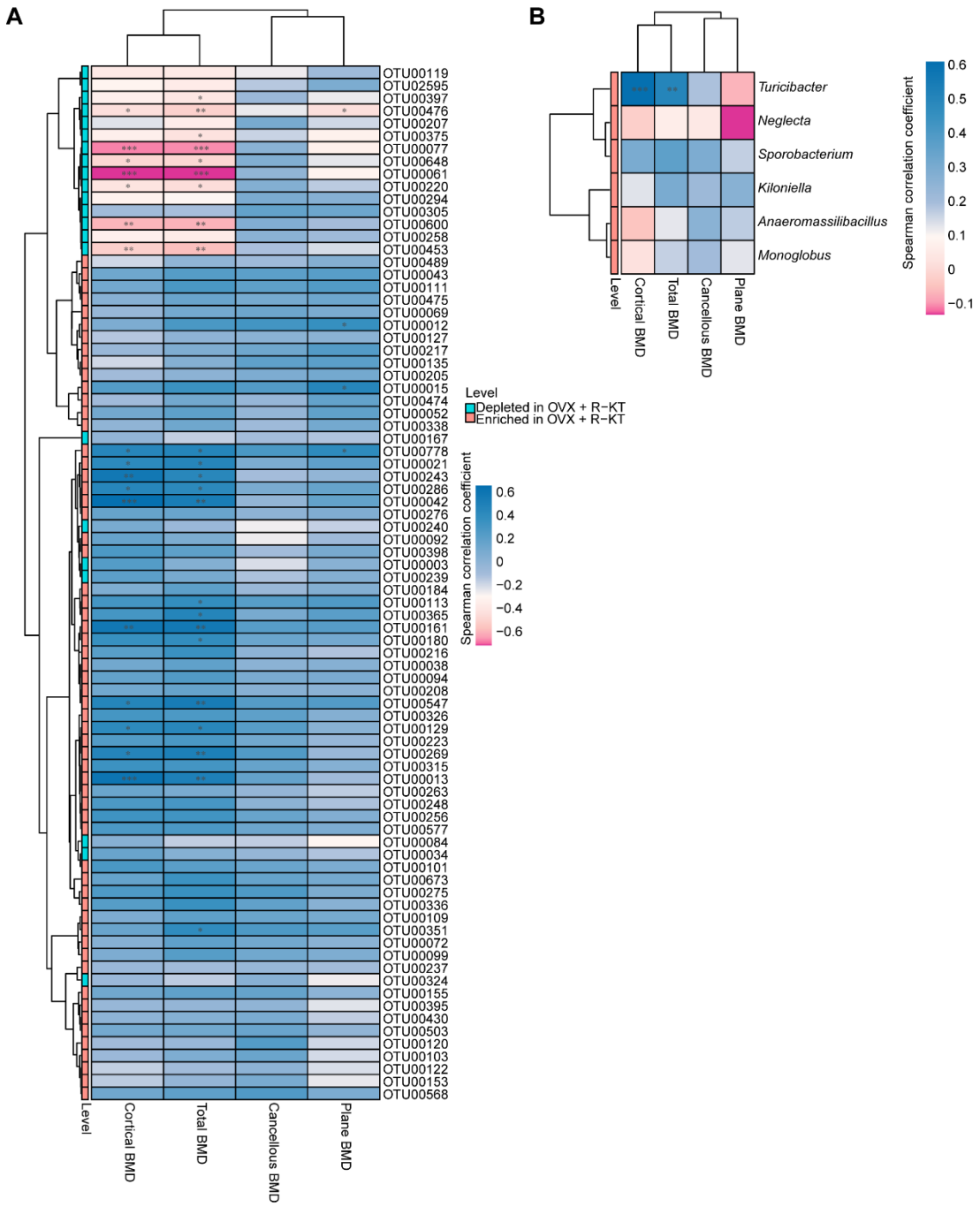

Figure 10. Spearman correlations between arketamine-associated gut microbiota and BMD

A: Correlations between representative OTUs with cortical BMD, total BMD, cancellous BMD and plane BMD of the mouse femur. B: Correlations between arketamine-related genera and cortical BMD, total BMD, cancellous BMD, and plane BMD of the mouse femur. *$P_{FDR} < 0.05$, **$P_{FDR} < 0.01$, ***$P_{FDR} < 0.001$. BMD: bone mineral density. OVX: ovariectomized. R-KT: arketamine.

3.2.4. Correlations of gut microbiota with SCFAs

We measured SCFAs in these fecal samples (**Supplementary Figure 2A**). There were significant changes in succinic acid among the three groups (Kruskal-Wallis rank test, P = 0.035). Levels of succinic acid in the OVX + arketamine group were significantly lower than those of sham + saline group. In contrast, there were no changes in other SCFAs (lactic acid, acetic acid, propionic acid, N-butyric acid, and N-valeric acid) among the three groups (**Supplementary Figure 2A**).

Interestingly, SCFAs were significantly associated with some OTUs. Spearman correlation network (absolute value of correlation coefficient > 0.6, P < 0.05) was shown in Supplementary Figure. 2B. Specifically, the concentration of succinic acid in mouse feces was negatively correlated with the abundance of the following 11 OTUs, such as OTU00041 (*Kineothrix*), OTU00056 (*Eisenbergiella*), OTU00072 (*Anaeromassilibacillus*), OTU00103 (*Faecalicatena*), OTU00146 (*Intestinimonas*), OTU00153 (*Neglecta*), OTU00189 (*Frisingicoccus*), OTU00194 (*Lachnoclostridium*), OTU00218 (*Breznakia*), OTU00309 (*Blautia*), and OTU00430 (*Roseburia*) (**Supplementary Figure 2B**). In contrast, there was a positive correlation between *OTU00003* (*Lactobacillus*) and succinic acid (**Supplementary Figure 2B**). Lactic acid was positively correlated with the abundance of OTU00104 (*Anaerocolumna*), and acetic acid was correlated with the relative abundance of OTU00020 (*Bifidobacterium*), OTU00216 (*Colidextribacter*), OTU00361 (*Anaerotignum*), OTU00365 (*Erysipelatoclostridium*), and OTU00457 (*Eubacterium*). Propionic acid was correlated with the abundance of OTU00457 (*Eubacterium*), OTU00979 (*Bacteroides*), OTU01702 (*Barnesiella*), OTU02595 (*Prevotella*). N-valeric acid was positively correlated with the abundance of OTU00512 (*Roseburia*), but negatively correlated with the abundance of OTU00260 (*Streptococcus*) (**Supplementary Figure 2B**).

3.2.5. Metabolomic analysis of plasma samples

To examine the interaction between gut microbiota and host metabolism at the plasma metabolic level, we performed a non-targeted metabolomics analysis of plasma samples. After quality control and removal of low-abundance peaks, a total of 199 positive ion pattern features and 73 negative ion pattern features were identified. The OPLS-DA model was employed to represent the distribution of plasma metabolic components in the OVX + saline group and the OVX + arketamine group. The scatter plots of the scores of the two models are shown (**Supplementary Figure 3A and 3B**). After thresholding metabolites (VIP values > 0.3, Wilcoxon rank p values < 0.05, FDR < 0.51), we identified a total of 24 metabolites with significant abundance differences between the OVX + saline group and OVX + arketamine group (**Figure 11A**). Includes 15 features that can be classified based on the data Human Metabolome Database and 9 features that cannot be classified (**Supplementary Table 2**). Specifically, 17 metabolites were downregulated in the OVX + arketamine group versus the OVX + saline group. These metabolites were [(Aminocarbonyl)(methyl)amino]acetic acid, 2,4-dichloro-5-ethyl-3-methylphenol, 2,5-dimethylthiazole, 2-aminoethylphosphonate, 2-methyl-1-butanethiol, 2-vinylthiophene, 3-methylthiophene, 9,10-dihydrojasmonic acid, D-alanine, dihydrouracil, DL-arginine, ethyl 3-mercaptobutyrate, ethyl 4-hydroxy-2-methyl-6-quinolinecarboxylate, L-citrulline, *N*-carbamoyl-glutamic acid, *N*-nitroethanediamine, xi-2-mercapto-3-methyl-1-butanol (**Figure. 11A**). In contrast, a total of 7 plasma metabolites were upregulated in the OVX + arketamine group compared to the OVX + saline group. These metabolites included 1,2,5-oxadiazole-3,4-dicarboxylic acid, 3-(3-acetyl-2,6-dihydroxy-5-methylbenzyl)-4-hydroxy-5-methylfuran-2(5H)-one, 4-deoxyerythronic acid, 5-[(4-nitrobenzoyl)amino] isophthalic acid, 5-keto-D-gluconic acid, citric acid, dihydroxyacetone (**Figure 11A**). Furthermore, we depicted the abundance distribution of these metabolites across the three groups (**Supplementary Figure 4**).

Next, we investigated the correlations between the above identified metabolites and BMD. A total of 9 plasma metabolites were significantly associated with BMD indices in mice (**Figure 11B**). Among them, 8 plasma metabolites, such as ethyl 4−hydroxy−2−methyl−6−uinolinecarboxylate, dihydrouracil,

2,4−dichloro−5−ethyl−3−methylphenol, 2−aminoethylphosphonate, 2,5−dimethylthiazole, 3−methylthiophene, 2−vinylthiophene, and *N*−carbamoyl-glutamic acid, were negatively correlated with the cortical BMD or total BMD (**Figure 11B**). These metabolites were classified into organic phosphonic acids, heteroaromatic compounds, pyrimidines and pyrimidine derivatives etc. In contrast, 5−[(4−nitrobenzoyl)amino]isophthalic acid was positively correlated with total BMD (**Figure 11B**).

These data suggest that metabolites including SCFAs may play a role in the beneficial effects of arketamine on the reduced BMD of OVX mice.

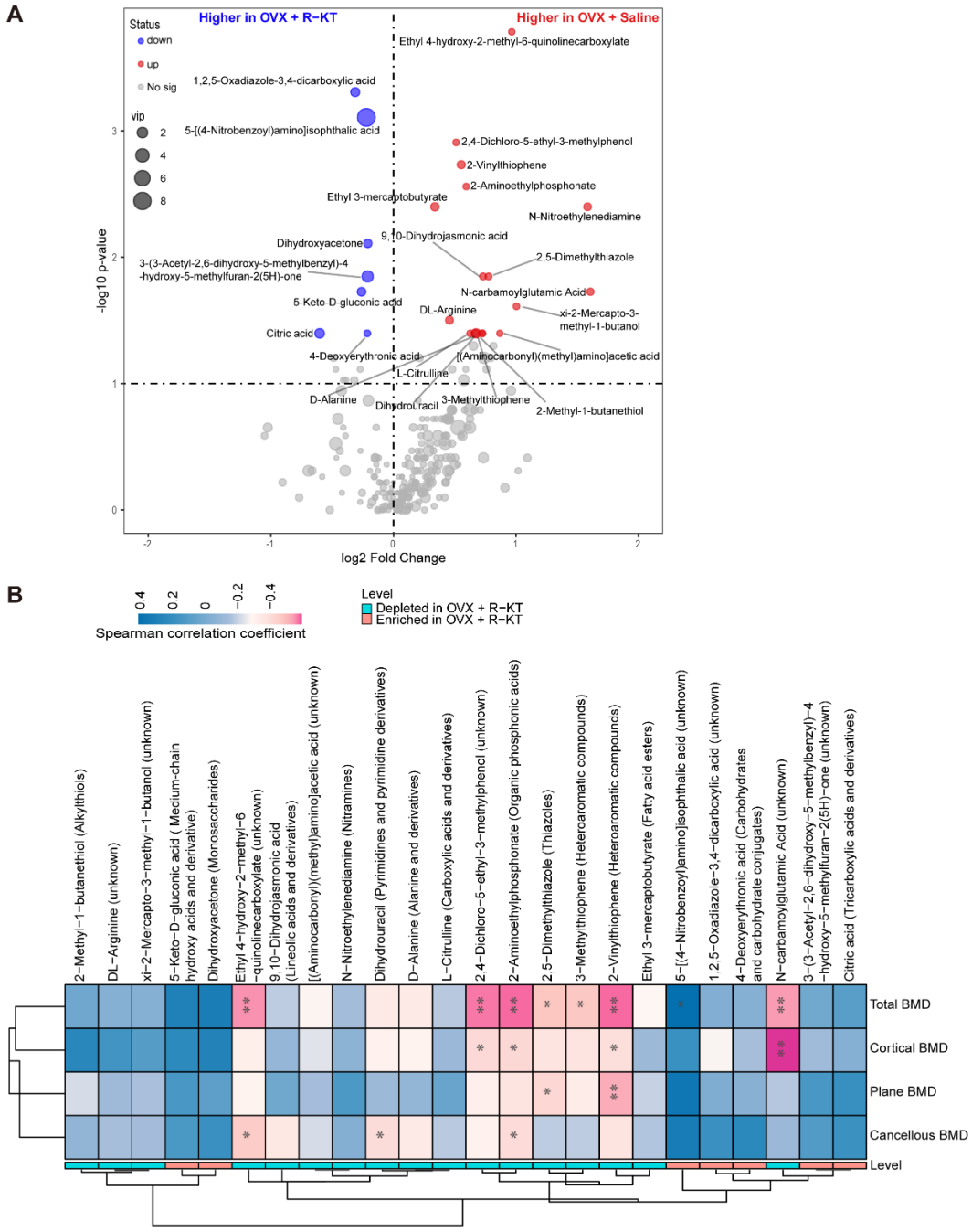

Figure 11. Plasma metabolomic changes between OVX + saline group and OVX + arketamine group and Spearman correlations between metabolites and femoral BMD

A: Volcano plots show the metabolite changes between OVX + saline group and OVX + arketamine group. X-axis indicates the log2-transformed plasma metabolite abundance of fold change, and the y-axis indicates the -log10-transformed p value using the Wilcoxon rank sum test. Horizontal lines indicate $p < 0{\cdot}05$. Increased or decreased metabolites are marked in red and blue, respectively. The size of the dot represents the size of VIP (variable importance in projection) value. Metabolites with $P < 005$ and $VIP > 0{\cdot}3$ are marked in text. B: Correlations between arketamine-associated metabolites with cortical BMD, total BMD, cancellous BMD and plane BMD of the mouse

femur. *P < 0.05, **P < 0.01, ***P < 0.001. BMD: bone mineral density. OVX: ovariectomized. R-KT: arketamine.

3.2.6. Relationships between gut microbiota and plasma metabolites

Finally, we analyzed the Spearman correlation between arketamine-associated microbiome and plasma metabolites (**Supplementary Figure 5**). There were Spearman correlations between the taxa and plasma metabolites (**Supplementary Figure 5**). A total of 14 arketamine-related OTUs (relative abundance > 0.1%) were significantly associated with 24 plasma metabolites (Spearman absolute rho > 0.5, P < 0.05), which were further related to mouse femoral BMD indices (**Figure 12A**). More specifically, succinic acid, and 2 OTUs [OTU00003 (*Lactobacillus*), and OTU00094 (*Eubacterium*)], as well as 2 plasma metabolites (1,2,5-oxadiazole-3,4-dicarboxylic acid and ethyl 4−hydroxy−2−methyl−6−uinolinecarboxylate) were significantly associated. Plasma metabolite ethyl 4−hydroxy−2−methyl−6−uinolinecarboxylate was negatively associated with total BMD. In addition, N-laveric acid was associated with OTU00042 (*Eisenbergiella*), which was associated with the arketamine-depleted metabolite *N*-carbamoyl-glutamic acid. *N*-carbamoyl-glutamic acid was negatively associated with cortical BMD and total BMD. More importantly, arketamine-enriched genera OTU00013 (*Turicibacter*) and OTU00042 (*Eisenbergiella*) were positively associated with both cortical BMD and total BMD, while arketamine-depleted genus OTU00061 (*Kineothrix*) was negatively correlated with cortical BMD and total BMD.

At the plasma metabolite level, five arketamine-depleted metabolites, N-carbamoyl-glutamic acid (unknown), ethyl 4-hydroxy-2-methyl-6-quinolinecarboxylate (unknown), 2-vinylthiophene (heteroaromatic compounds), 2-aminoethylphosphonate (organic phosphonic acids), and 2,4-dichloro-5-ethyl-3-methylphenol (unknown) were directly or indirectly negatively associated with BMD (**Figure 12A**). The relative abundances of the identified flora and metabolites that were associated with BMD in the OVX mice across different groups are shown (**Figure 12B and 12C**).

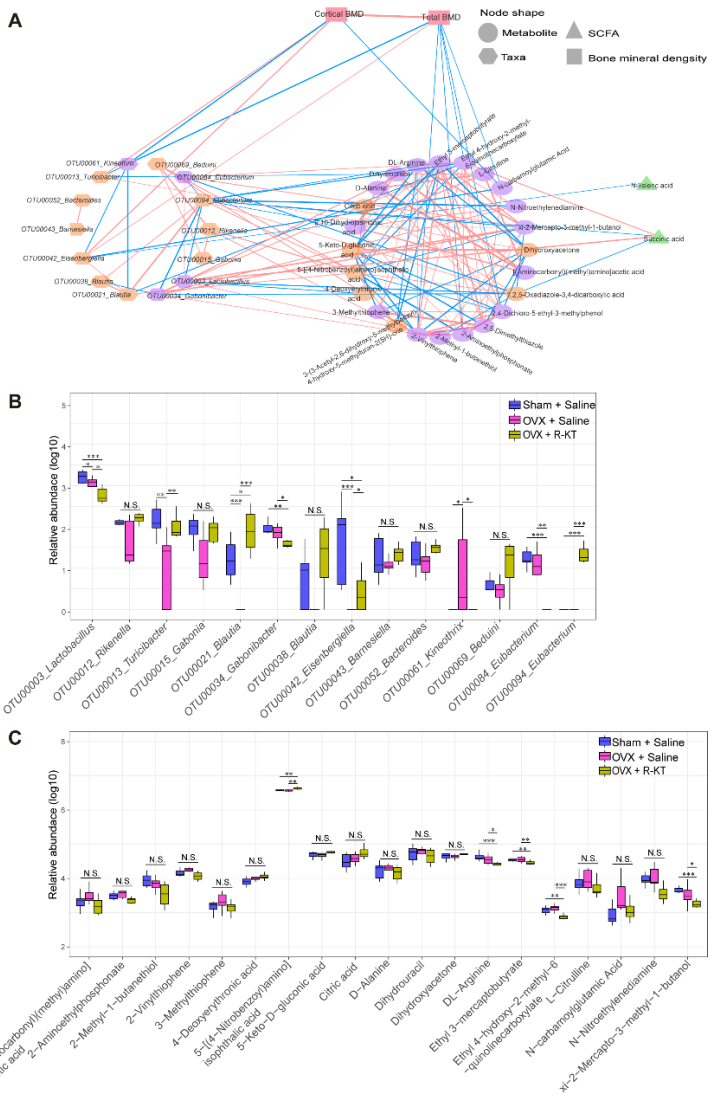

Figure 12. An integrated association network reflecting host-microbe interactions, relative abundance and metabolic characteristics of key arketamine-related OTUs in different groups

A: Network plots were used to investigate arketamine-associated flora (relative abundance > 0.1%), arketamine-associated metabolites ($P_{FDR} < 0.05$, VIP > 0.3, OVX + saline group vs. OVX + R-KT group), and the interrelationship of fecal SCFAs, and their relationship with mouse femoral BMD index. Red connections indicate positive correlations, blue connections indicate negative correlations, and thicker connection lines indicate larger correlation coefficients (Spearman correlation analysis, absolute value of correlation coefficient > 0.5, $P_{FDR} < 0.05$). The red square nodes represent the BMD index, the hexagonal nodes represent the intestinal flora, the circular nodes represent the plasma metabolites, orange indicates arketamine enriched OTUs or metabolites, purple indicates arketamine depleted OTUs or metabolites, the green triangular nodes represent the short chain fatty acids in feces. B: Changes in important OTUs associated with arketamine in the three groups. C: Changes in important arketamine-related metabolic profiles in the three groups. Wilcoxon Rank sum test. *$P_{FDR} < 0.05$, **$P_{FDR} < 0.01$, ***$P_{FDR} < 0.001$. BMD, bone mineral density. R-KT: arketamine. VIP, variable importance in projection. SCFAs, short-chain fatty acids.

3.2.7. Predicted functional pathway analysis

Prediction of metagenomic function was achieved using the PICRUSt2 tool based on the MetaCyc database. In this study, a total of 27 pathways with different abundance between the OVX + saline group and the OVX + arketamine group ($P < 0.05$, FDR < 0.3, difference between means > 0.02) (Supplementary Figure. 6). In the OVX + arketamine group, a total of five pathways such as glycerol degradation to butanol, L-methionine biosynthesis III, cob(II)yrinate a,c-diamide biosynthesis I (early cobalt insertion), L-lysine fermentation to

acetate and butanoate, and superpathway of fucose and rhamnose degradation were enriched (**Supplementary Figure 6**). In contrast, a total of 22 pathways were reduced in the OVX + arketamine group. These pathways included hexitol fermentation to lactate, formate, ethanol and acetate, superpathway of N-acetylneuraminate degradation, superpathway of glycolysis and the Entner-Doudoroff pathway, superpathway of pyrimidine nucleobases salvage, pyruvate fermentation to acetate and lactate II, guanosine ribonucleotides *de novo* biosynthesis, phosphatidylglycerol biosynthesis II (non-plastidic), phosphatidylglycerol biosynthesis I (plastidic), UDP-N-acetylmuramoyl-pentapeptid biosynthesis I, peptidoglycan biosynthesis III (mycobacteria), peptidoglycan biosynthesis I, superpathway of phospholipid biosynthesis I (bacteria), S-adenosyl-L-methionine cycleI, UMP biosynthesis I, UDP-*N*-acetylmuramoyl-pentapeptide biosynthesis II, adenosine ribonucleotides de novo biosynthesis, D-galactose degradation I (Leloir pathway), coenzyme A biosynthesis I (prokaryotic), glycolysis III (from glucose), L-lysine biosynthesis VI, L-lysine biosynthesis III, and tRNA charging pathway (**Supplementary Figure 6**).

4. Discussion

The main findings of our study were as follows. First, a single dose of arketamine improved the anhedonia-like behavior and reduced cortical (and total) BMD in the CSDS susceptible mice, consistent with a previous report (Xiong et al., 2019). Positive correlations were found between sucrose preference and cortical and total BMD, suggesting a relationship between anhedonia-like behavior and reduced BMD in CSDS susceptible mice. Second, repeated intermittent administration of arketamine could attenuate the reduction of cortical BMD and total BMD of the OVX mice, consistent with our previous report (Fujita and Hashimoto, 2020). Third, α- and β-diversity differed significantly among the three groups in CSDS model and OVX model. Fourth, significant differences were observed in the abundance of gut microbiota between the CSDS + saline and CSDS + arketamine groups or OVX + saline group and the OVX + arketamine group. Fifth, untargeted metabolomics analysis identified six altered metabolites in the CSDS + arketamine group compared with the CSDS + saline group. Sixth, in the CSDS model, there were correlations of the abundance of certain metabolites (and microbiota) with anhedonia-like behavior and cortical (and total) BMD in the control, CSDS + saline, and CSDS + arketamine groups. In the OVX model, there were positive correlations between the genera *Turicibacter* (and several metabolites) and cortical (or total) BMD. Collectively, these data suggest that gut microbiota and microbiome-derived metabolites may play a role in the ability of arketamine to improve the reduced BMD of CSDS susceptible mice and OVX mice.

The α-diversity of the gut microbiota was significantly higher in the CSDS + saline group than control group, suggesting a significant effect of CSDS on the composition of the gut microbiota. Furthermore, α-diversity (i.e., observed_OTUs, and ACE) of gut microbiota in OVX + arketamine group was significantly higher than that in OVX + saline group, indicating that arketamine had a significant effect on gut microbiota composition of OVX mice. In both CSDS model and OVX model, the comparison of β-diversity among the three groups indicated that arketamine could contribute to structural dissimilarity among gut microbial communities. Previous studies showed that the abnormal gut microbiota composition seen in CSDS susceptible mice was ameliorated by a single dose of arketamine (10 mg/kg) (Qu et al., 2017). In addition, a single dose of arketamine significantly alleviated the decreases in cortical and total BMD seen in CSDS susceptible mice (Xiong et al., 2019). Collectively, the results suggest that a single dose of arketamine influences the altered gut microbiota composition that characterizes CSDS susceptible mice and OVX mice,

and that normalization of abnormal composition of gut microbiota by arketamine may play a role in the beneficial effects on reduced BMD of CSDS susceptible mice and OVX mice.

In the CSDS model, we found a negative correlation between the abundance of *Lactobacillus taiwanensis* and cortical BMD in the control and CSDS + saline groups, although there were positive correlations between the abundances of four species microbiota and total BMD in both groups. Taken together, the data suggest that alterations in the abundance of these microbiota may be involved in the reduced BMD seen in CSDS susceptible mice, although further study is needed to confirm this.

In the OVX model, the phylum *Tenericutes* was significantly reduced in OVX + arketamine group. The phylum *Tenericutes* was more abundant in treatment-resistant patients with depression (Fontana et al., 2020), suggesting that *Tenericutes* may be involved in the dysbiosis of the gut microbiota in severe depression. The abundance of *Tenericutes* was positively associated with pro-inflammatory cytokines (IL-6 and TNF-α), but negatively related with insulin treatment in diabetic mice (Li et al., 2019). Since bone loss is associated with inflammation, the potential mechanism for the hemophilic arthropathy induced bone loss may be the activation of TNF-α-dependent osteoclastogenesis (Haxaire et al., 2018). Taken together, arketamine may remodel the pro-inflammatory intestinal microenvironment, resulting in the maintenance of intestinal homeostasis. The genus *Anaeromassilibacillus* was initially isolated and identified from the stool of a child with kwashiorkor (Guilhot et al., 2016). Zinc deficiency has been associated with depression in humans and animal models of depression. In pregnant mice on a zinc inhibitor diet, the abundance of *Kiloniella* was significantly decreased, accompanied by activation of inflammatory signaling (Sauer and Grabrucker, 2019). In this study, we found that high abundance of *Kiloniella* was observed in arketamine + OVX group, suggesting that arketamine may suppress inflammatory processes by regulating the composition of intestinal flora. Changes in the genus *Turicibacter* abundance have been associated with diseases including inflammation and colon cancer (Zackular et al., 2013). Furthermore, *Turicibacter sanguinis* colonization has been reported to modulate intestinal lipid metabolism and systemic triglyceride profiles in mice, which may be related to the relationship between SSRI use and metabolic syndrome symptoms (Fung et al., 2019). Collectively, the alterations of gut microbiota in OVX + arketamine group are likely involved in the beneficial effects of arketamine on reduced BMD of OVX mice, although further studies are required to determine detailed mechanisms of gut microbiota in postmenopausal osteopenia.

Circulating biomarkers are becoming clinically reliable indicators of the status of bone metabolism. Metabolomics provides a new platform for screening novel biomarkers for various metabolic diseases, such as osteoporosis and diabetes (Wang et al., 2011; Yang et al., 2020). Arketamine-depleted metabolite 3-methylthiophene was negatively associated with BMD of mice, which belongs to a group of organic compounds known as heteroaromatic compounds, exhibited dose-dependent cytotoxic effects against breast cancer cell lines (Baig et al., 2016). De Preter et al. (De Preter et al., 2015) reported higher levels of 3,4-dimethylthiophene in stool samples from patients with Crohn's disease than in healthy controls, indicating that it is an important metabolic biomarker of the changes associated with inflammatory bowel disease. In our study, we detected lower plasma levels of 3-methylthiophene in OVX + arketamine mice than in OVX mice, and it was significantly negatively correlated with total BMD of the mice, suggesting that arketamine may play a role in regulating plasma metabolites to improve the inflammatory state. In addition, we found arketamine-depleted plasma metabolite dihydrouracil, an intermediate decomposition product of uracil. Altered levels of dihydrouracil are usually associated with metabolic disorders. Patients with

dihydropyrimidine enzyme deficiency have elevated levels of dihydrouracil and exhibit various neurological abnormalities, autistic behavior, and gastrointestinal dysfunction (gastroesophageal reflux, recurrent vomiting) (Liu et al., 2014). Collectively, these metabolites might play a role in the beneficial effects of arketamine in OVX mice. In the CSDS model, we found positive correlations between sucrose preference (in the SPT) and BMD in all three groups, suggesting an inverse relationship between the severity of the anhedonia-like phenotype and BMD. A meta-analysis showed that the BMD of the hip is reduced in older adults with depression (Stubbs et al., 2016). In a population-based study, the depression score was a significant predictor of the BMD of the lumbar spine and total hip in a cohort of 465 older adults (aged $\geq$ 60 years) (Hlis et al., 2018), suggesting that depression is a risk factor for osteoporosis and fractures in elderly people. A pilot study demonstrated that a single intravenous infusion of arketamine (0.5 mg/kg) exerted rapid-onset and sustained antidepressant effects in treatment-resistant patients with MDD (Leal et al., 2021). Our current study reported that repeated intermittent administration of arketamine ameliorated the decreases in cortical and total BMD in the OVX mice. Given the close relationship between depression and reduced BMD in the elderly, arketamine could ameliorate this BMD reduction in elderly people with MDD, and it would be a suitable antidepressant without the risk of fractures.

Patients with major depression are associated with low BMD, suggesting a risk for osteoporosis (Cizza et al., 2010). A study using a population-based sample demonstrated that depression score was a significant predictor of BMD at the lumbar spine and total hip in older participants (Hlis et al., 2018). Although decreased BMD in patients with depression is well recognized, bone loss in patients with depression is not treated adequately. It is likely that arketamine may ameliorate reduced BMD in elderly people with depression.

5. Conclusion

In conclusion, this study showed that a single administration of arketamine can attenuate the anhedonia-like behavior and reduction of BMD in CSDS susceptible mice. Repeated intermittent administration of arketamine could attenuate OVX-induced reduction of BMD in mice. Furthermore, this study suggests that gut microbiota, microbes-derived metabolites may be involved in the beneficial effects of arketamine on reduced BMD and anhedonia-like behavior, implying a role of the gut–microbiota–bone–brain axis. Therefore, it is of great interest whether arketamine could improve reduced BMD and depressive symptoms in patients with osteoporosis or depression.

Supplemental material

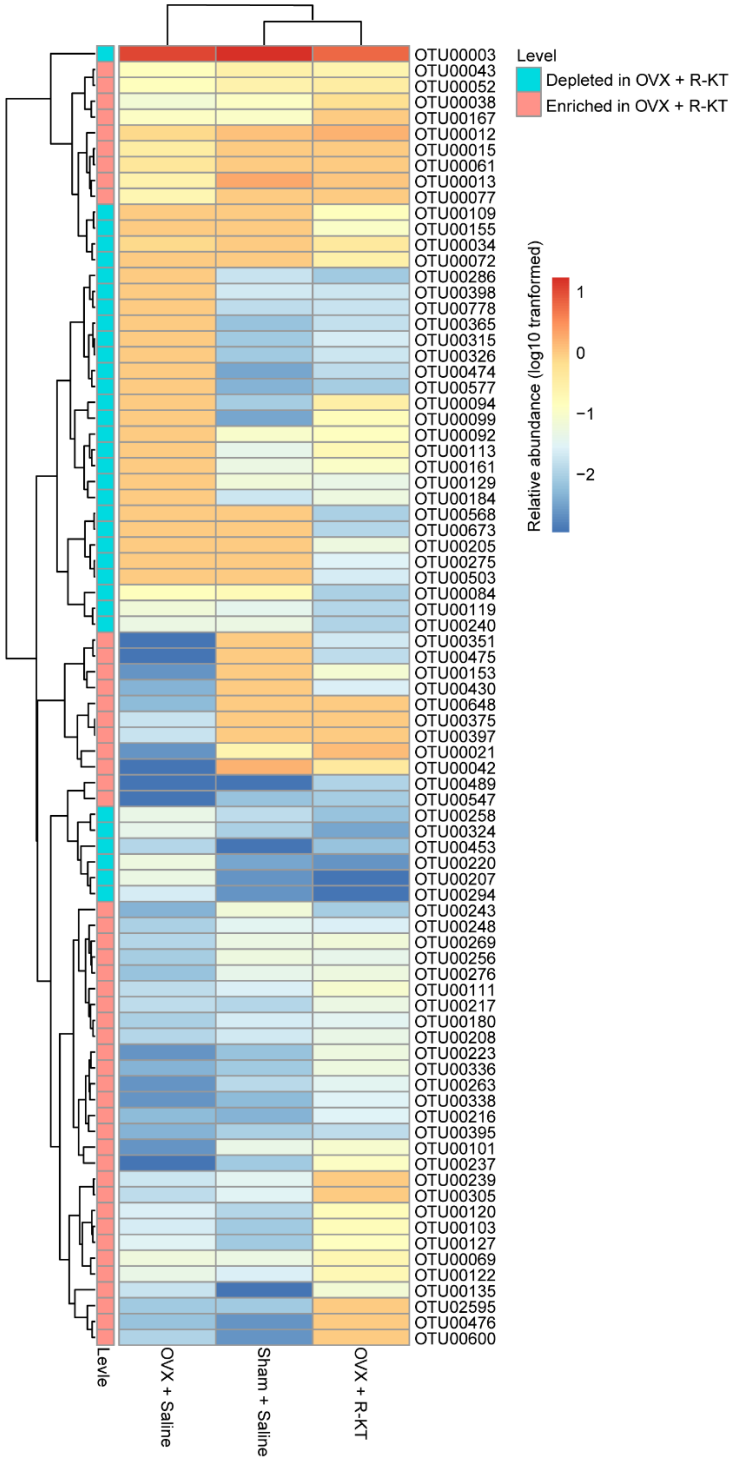

Supplemental Figure 1. Heatmap of the relative abundance of differential OTUs in the three groups

Relative abundance of (*R*)-ketamine-associated differential OTUs in sham + saline group, OVX + saline group and OVX + arketamine group. OVX: ovariectomized. R-KT: arketamine.

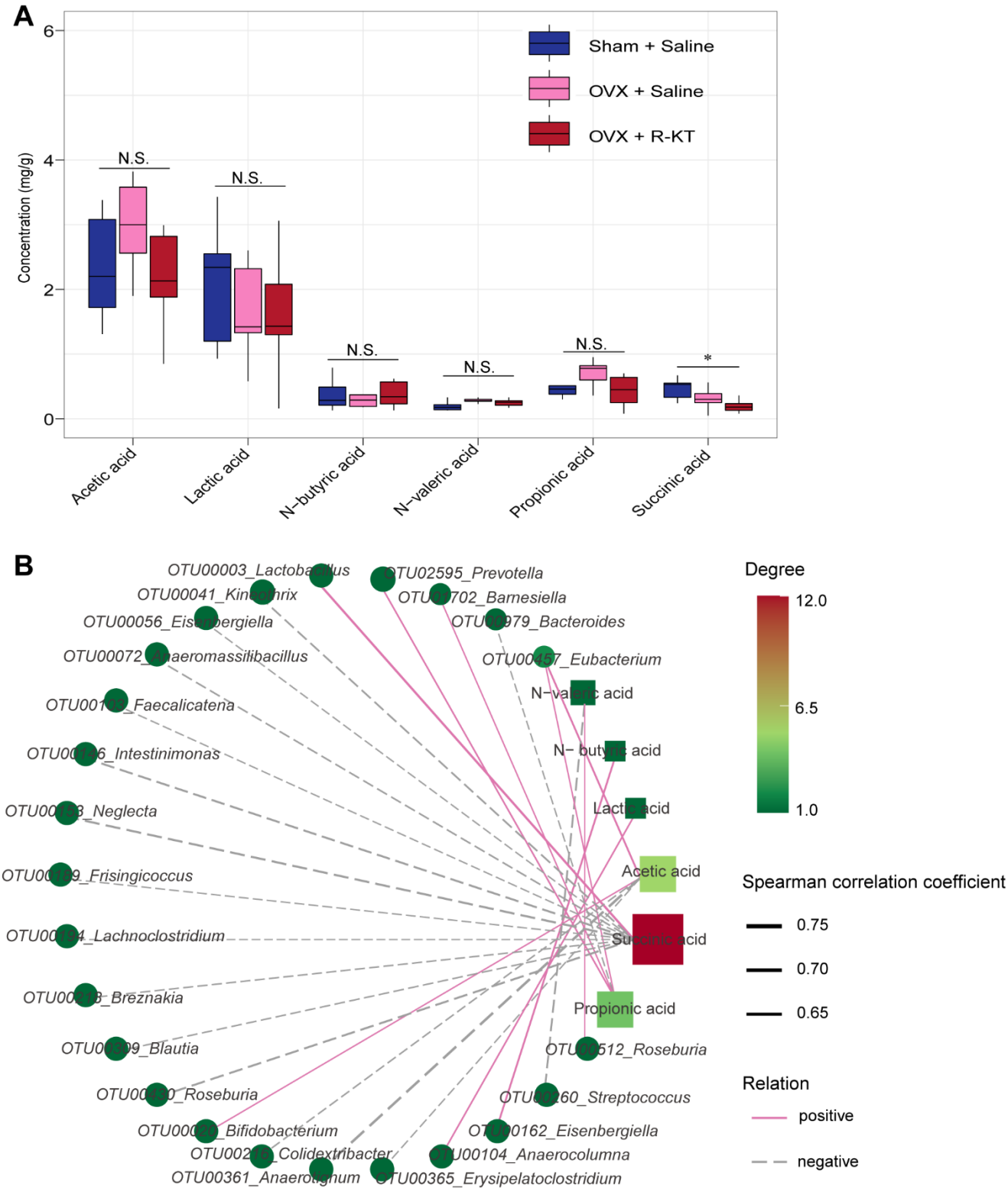

Supplemental Figure 2. Fecal SCFAs in the three groups and spearman correlations between SCFAs and relative abundance of gut microbiota

A: The concentration of succinic acid was significantly lower in the OVX + R-KT group than that of sham + saline group (Kruskal-Wallis test; P = 0.01). In contrast, there was no differences in other SCFAs (acetic acid, lactic acid, N-butyric acid, N-valeric acid and propionic acid) among the three groups. B: Spearman's correlation network between fecal SCFAs concentration and relative abundance of intestinal flora (absolute correlation coefficient > 0.6, $P_{FDR} < 0.05$). Red solid lines represent positive correlations, gray dashed lines represent negative correlations, and thicker lines represent larger correlations. Round nodes represent intestinal flora, square nodes represent SCFAs, larger nodes mean more nodes are correlated with them. *P < 0.05, N.S., not significant. SCFAs, short chain fatty acids. OVX: ovariectomized. R-KT: arketamine.

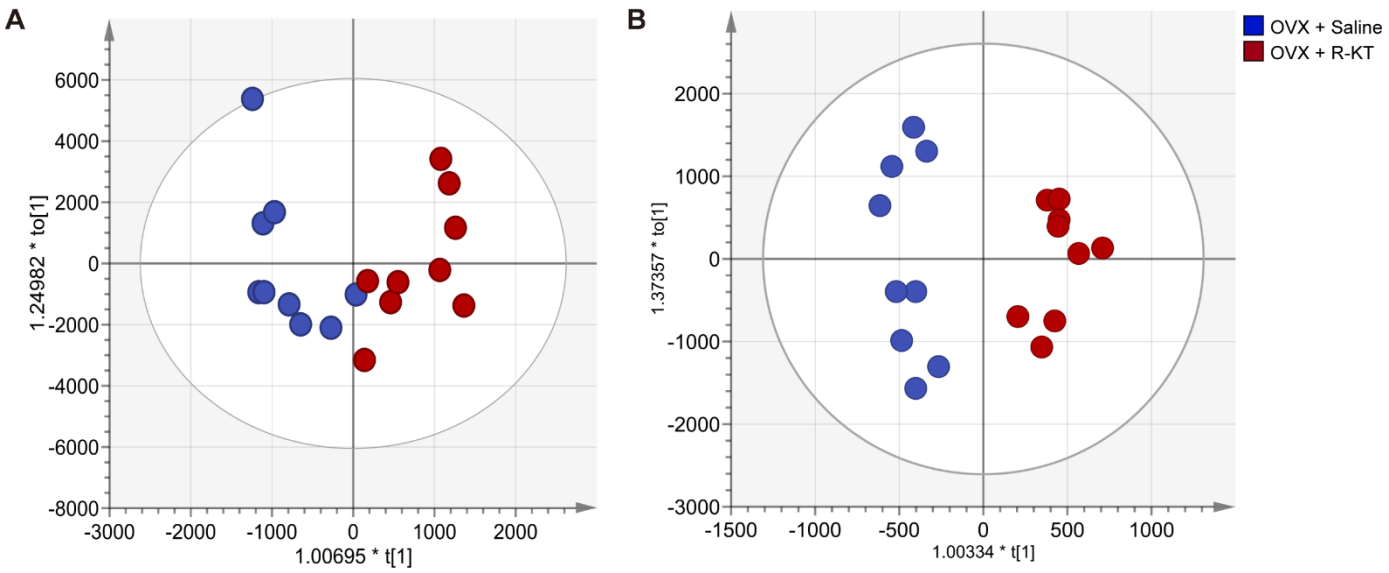

Supplemental Figure 3. Scatter plot of mouse plasma metabolites based on orthogonal partial least square discriminant analysis (OPLS-DA) between OVX + saline group and OVX + R-KT group

A: Positive ion mode. B: Negative ion mode. OVX: ovariectomized. R-KT: arketamine.

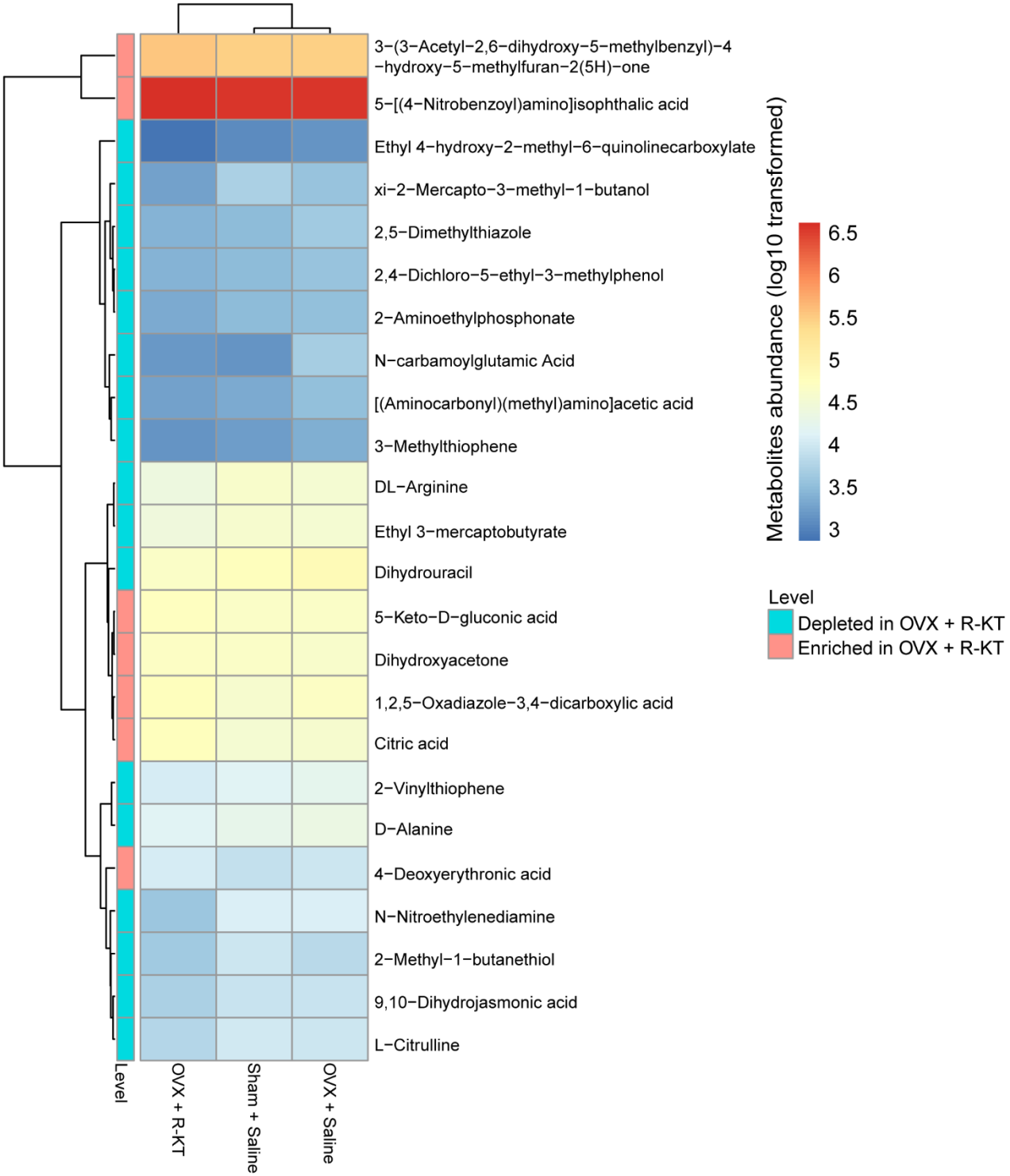

Supplemental Figure 4. Heatmap of the relative abundance of differential metabolites in the three groups

Abundance of differential metabolites between the OVX + saline group and the OVX + R-KT group across samples. OVX: ovariectomized. R-KT: arketamine.

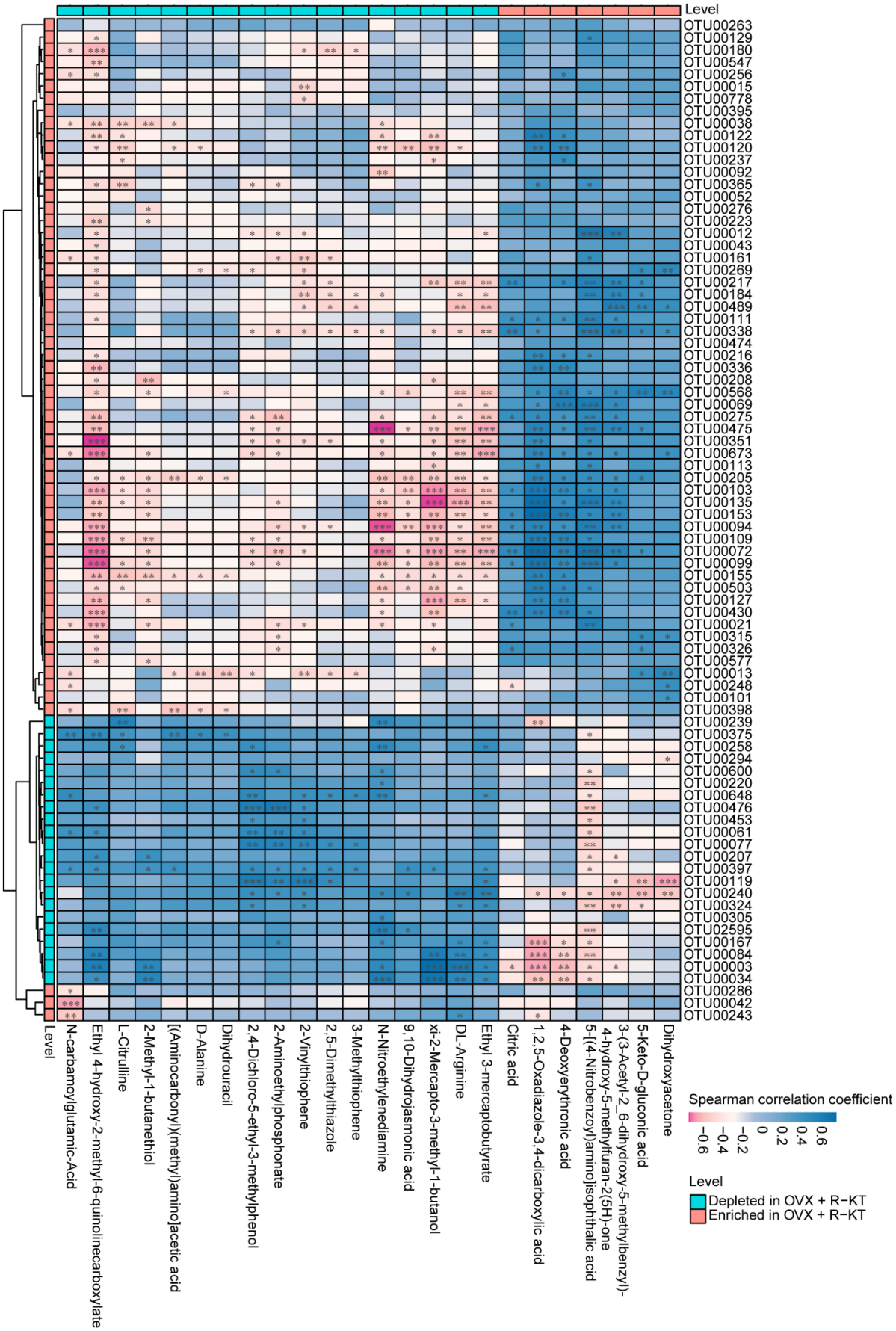

Supplemental Figure 5. Associations of arketamine-related bacteria and metabolites.

The heatmap describes Spearman correlations between arketamine-related bacteria and plasma metabolites. *$P_{FDR} < 0.05$, **$P_{FDR} < 0.01$, ***$P_{FDR} < 0.001$. OVX: ovariectomized. R-KT: arketamine.

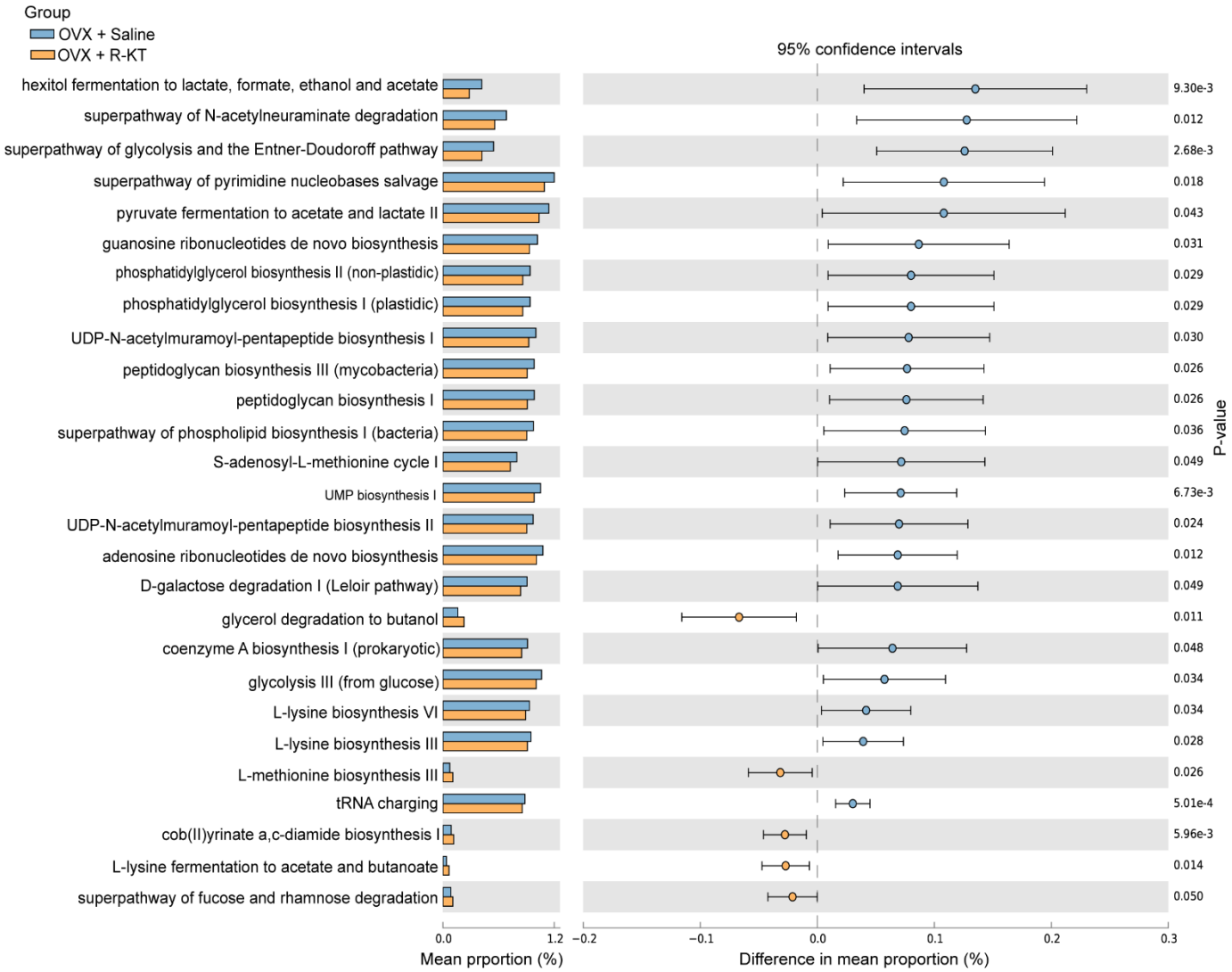

Supplemental Figure 6. The proportion of function predicted for the MetaCyc pathway differed between the OVX + saline and OVX + R-KT groups.

Bar graphs show the average proportion of different pathways in Metacyc predicted using PICRUST2. Differences in between-group ratios are shown within the 95% confidence limits. OVX: ovariectomized. R-KT: arketamine.

Supplemental Table 1. The OTUs and genera were differentially abundant between OVX + saline group and OVX + R-KT group.

OTUID	Mean relative abundance (%)		Wilcoxon rank-sum test	Levels
	OVX + Saline	OVX + R-KT	P-value	
OTU00012	0.754	1.627	0.024	
OTU00013	0.247	1.133	0.002	
OTU00015	0.357	0.993	0.017	
OTU00021	0.002	1.314	0.000	
OTU00038	0.077	0.610	0.005	
OTU00042	0.001	0.401	0.014	
OTU00043	0.142	0.243	0.017	
OTU00052	0.150	0.338	0.019	
OTU00069	0.062	0.203	0.037	
OTU00072	0.000	0.279	0.000	
OTU00092	0.000	0.130	0.002	
OTU00094	0.000	0.324	0.001	
OTU00099	0.000	0.158	0.000	
OTU00101	0.002	0.089	0.018	
OTU00103	0.022	0.160	0.003	
OTU00109	0.000	0.140	0.002	
OTU00111	0.014	0.090	0.004	
OTU00113	0.000	0.191	0.005	
OTU00120	0.024	0.163	0.023	
OTU00122	0.044	0.186	0.015	
OTU00127	0.031	0.129	0.015	
OTU00129	0.000	0.044	0.014	
OTU00135	0.017	0.071	0.005	Enriched in OVX + R-KT
OTU00153	0.002	0.081	0.002	
OTU00155	0.000	0.107	0.005	
OTU00161	0.000	0.110	0.002	
OTU00180	0.010	0.034	0.020	
OTU00184	0.000	0.053	0.002	
OTU00205	0.000	0.054	0.005	
OTU00208	0.012	0.047	0.011	
OTU00216	0.006	0.029	0.020	
OTU00217	0.014	0.049	0.020	
OTU00223	0.002	0.058	0.023	
OTU00237	0.001	0.120	0.040	
OTU00243	0.004	0.009	0.023	
OTU00248	0.010	0.027	0.011	
OTU00256	0.009	0.040	0.016	
OTU00263	0.002	0.033	0.013	
OTU00269	0.012	0.069	0.001	
OTU00275	0.000	0.028	0.014	
OTU00276	0.007	0.057	0.033	
OTU00286	0.000	0.008	0.033	
OTU00315	0.000	0.022	0.014	
OTU00326	0.000	0.019	0.005	
OTU00336	0.004	0.053	0.001	

OTU00338	0.002	0.028	0.021	
OTU00351	0.001	0.021	0.019	
OTU00365	0.000	0.016	0.002	
OTU00395	0.004	0.014	0.040	
OTU00398	0.000	0.019	0.014	
OTU00430	0.004	0.024	0.011	
OTU00474	0.000	0.014	0.013	
OTU00475	0.001	0.014	0.005	
OTU00489	0.001	0.011	0.033	
OTU00503	0.000	0.023	0.005	
OTU00547	0.001	0.009	0.021	
OTU00568	0.000	0.010	0.014	
OTU00577	0.000	0.009	0.014	
OTU00673	0.000	0.012	0.005	
OTU00778	0.000	0.017	0.014	
OTU00003	11.093	6.099	0.011	Depleted in OVX + R-KT
OTU00034	0.763	0.434	0.022	
OTU00061	0.470	0.000	0.001	
OTU00077	0.207	0.000	0.002	
OTU00084	0.142	0.010	0.014	
OTU00119	0.066	0.012	0.005	
OTU00167	0.117	0.000	0.005	
OTU00207	0.050	0.001	0.005	
OTU00220	0.057	0.002	0.008	
OTU00239	0.019	0.000	0.034	
OTU00240	0.050	0.011	0.006	
OTU00258	0.047	0.007	0.027	
OTU00294	0.022	0.001	0.016	
OTU00305	0.014	0.000	0.014	
OTU00324	0.041	0.003	0.016	
OTU00375	0.018	0.000	0.014	
OTU00397	0.017	0.000	0.014	
OTU00453	0.012	0.007	0.025	
OTU00476	0.007	0.000	0.013	
OTU00600	0.011	0.000	0.002	
OTU00648	0.006	0.000	0.012	
OTU02595	0.008	0.000	0.001	
Genus				
Anaeromassilibacillus	0.26	0.82	0.008	Enriched in OVX + R-KT
Kiloniella	0.01	0.09	0.004	
Monoglobus	0.01	0.09	0.003	
Neglecta	0.01	0.16	0.003	
Sporobacterium	0.00	0.11	0.005	
Turicibacter	0.26	1.15	0.003	

Supplementary Table 2. Differential metabolites between OVX + saline group and OVX + R-KT group

Metabolite	Mean (OVX + Saline)	Mean (OVX + R-KT)	P-Value	FDR	VIP value	Status	HMDB ID	Classification
1,2,5-Oxadiazole-3,4-dicarboxylic acid	49602.421	61562.049	0.000	0.06	1.164		_	unknown
3-(3-Acetyl-2,6-dihydroxy-5-methylbenzyl)-4-hydroxy-5-methylfuran-2(5H)-one	310521.378	359228.111	0.014	0.31	2.386		_	unknown
4-Deoxyerythronic acid	9941.049	11526.316	0.040	0.50	0.373		HMDB0000498	Organic compounds (Sugar acids and derivatives)
5-[(4-Nitrobenzoyl)amino]isophthalic acid	3711124.778	4324832.000	0.001	0.07	8.612	Enriched in OVX + R-KT	_	unknown
5-Keto-D-gluconic acid	47609.623	57020.522	0.019	0.35	1.010		HMDB0011731	Organic compounds (Medium-chain hydroxy acids and derivatives)
Citric acid	40732.732	61827.284	0.040	0.50	1.450		HMDB0000094	Organic compounds (Tricarboxylic acids and derivatives)
Dihydroxyacetone	44206.864	51098.417	0.008	0.21	0.900		HMDB0001882	Organic compounds (Monosaccharides)
[(Aminocarbonyl)(methyl)amino]acetic acid	3381.263	1851.543	0.040	0.50	0.302		_	unknown
2,4-Dichloro-5-ethyl-3-methylphenol	3758.643	2636.255	0.001	0.08	0.352		_	unknown
2,5-Dimethylthiazole	4534.755	2647.165	0.014	0.31	0.437		HMDB0032975	Organic compounds (Thiazoles)
2-Aminoethylphosphonate	3515.372	2328.422	0.003	0.11	0.348	Depleted in OVX + R-KT	HMDB0011747	Organic compounds (Organic phosphonic acids)
2-Methyl-1-butanethiol	7223.923	4373.407	0.040	0.50	0.478		HMDB0035418	Organic compounds (Alkylthiols)
2-Vinylthiophene	17743.008	12087.646	0.002	0.10	0.823		HMDB0029726	Organic compounds (Heteroaromatic compounds)

3-Methylthiophene	2451.267	1480.409	0.040	0.50	0.313		HMDB0033119	Organic compounds (Heteroaromatic compounds)
9,10-Dihydrojasmonic acid	9130.455	5498.809	0.014	0.31	0.454		HMDB0033601	Fatty Acyls (Lineolic acids and derivatives)
D-Alanine	23962.956	15076.600	0.040	0.50	0.738		HMDB0001310	Organic acids and derivatives (Alanine and derivatives)
Dihydrouracil	74200.687	46485.143	0.040	0.50	1.333		HMDB0000076	Organoheterocyclic compounds (Pyrimidines and pyrimidine derivatives)
DL-Arginine	36068.180	26267.752	0.031	0.45	0.750		_	unknown
Ethyl 3-mercaptobutyrate	36075.363	28525.897	0.004	0.13	0.933		HMDB0032271	Fatty Acyls (Fatty acid esters)
Ethyl 4-hydroxy-2-methyl-6-quinolinecarboxylate	1498.478	767.078	0.000	0.04	0.313		_	unknown
L-Citrulline	10219.607	6620.457	0.040	0.50	0.364		HMDB0000904	Organic acids and derivatives (Carboxylic acids and derivatives)
N-carbamoylglutamic Acid	4938.954	1620.425	0.019	0.35	0.550		_	unknown
N-Nitroethylenediamine	12384.663	4129.189	0.004	0.13	0.687		HMDB0031226	Organic nitro compounds (Nitramines)
xi-2-Mercapto-3-methyl-1-butanol	3798.577	1893.381	0.024	0.40	0.373		_	unknown

Acknowledgements

This study was supported by the grant from Japan Agency for Medical Research and Development (to K.H., JP20dm0107119), Japan Society for the Promotion of Science (to K.H., 21H02846, 21H00184, 21H05612), JST OPERA Program Japan (to C.M JPMJOP1831) and unrestricted grant of Yamada Bee Company, Japan (to C.M).

Ms. Xiayun Wan was supported by the Academic Research & Innovation Management Organization of Chiba University (Chiba, Japan).

References

Agarwal, S., Germosen, C., Kil, N., Bucovsky, M., Colon, I., Williams, J., Shane, E., Walker, M.D., 2020. Current anti-depressant use is associated with cortical bone deficits and reduced physical function in elderly women. Bone 140, 115552.

Baig, U., Gondal, M.A., Alam, M.F., Wani, W.A., Younus, H., 2016. Pharmacological evaluation of poly(3-methylthiophene) and its titanium(IV)phosphate nanocomposite: DNA interaction, molecular docking, and cytotoxic activity. J. Photochem. Photobiol. B. 164, 244–255.

Chang, L., Wei, Y., Hashimoto, K., 2022. Brain-gut-microbiota axis in depression: A historical overview and future directions. Brain Res. Bull. 182, 44–56.

Cizza, G., Primma, S., Coyle, M., Gourgiotis, L., Csako, G., 2010. Depression and osteoporosis: a research synthesis with meta-analysis. Horm. Metab. Res. 42, 467–482.

Cizza, G., Primma, S., Csako, G., 2009. Depression as a risk factor for osteoporosis. Trends Endocrinol. Metab. 20, 367–373.

De Preter, V., Machiels, K., Joossens, M., Arijs, I., Matthys, C., Vermeire, S., Rutgeerts, P., Verbeke, K., 2015. Faecal metabolite profiling identifies medium-chain fatty acids as discriminating compounds in IBD. Gut 64, 447–458.

Douglas, G.M., Maffei, V.J., Zaneveld, J.R., Yurgel, S.N., Brown, J.R., Taylor, C.M., Huttenhower, C., Langille, M., 2020. PICRUSt2 for prediction of metagenome functions. Nat. Biotechnol. 38(6), 685–688.

Fan, Y., Pedersen, O., 2021. Gut microbiota in human metabolic health and disease. Nat. Rev. Microbiol. 19, 55–71.

Fontana, A., Manchia, M., Panebianco, C., Paribello, P., Arzedi, C., Cossu, E., Garzilli, M., Montis, M.A., Mura, A., Pisanu, C., Congiu, D., Copetti, M., Pinna, F., Carpiniello, B., Squassina, A., Pazienza, V., 2020. Exploring the role of gut microbiota in major depressive disorder and in treatment resistance to antidepressants. Biomedicines 8, 311.

Fujita, Y., Hashimoto, K., 2020. Decreased bone mineral density in ovariectomized mice is ameliorated after subsequent repeated intermittent administration of (*R*)-ketamine, but not (*S*)-ketamine. Neuropsychopharmacol. Rep. 40, 401–406.

Fung, T.C., Vuong, H.E., Luna, C., Pronovost, G.N., Aleksandrova, A.A., Riley, N.G., Vavilina, A., McGinn, J., Rendon, T., Forrest, L.R., Hsiao, E.Y., 2019. Intestinal serotonin and fluoxetine exposure modulate bacterial colonization in the gut. Nat. Microbiol. 4, 2064–2073.

Guilhot, E., Tidjani Alou, M., Diallo, A., Raoult, D., Khelaifia, S., 2016. *Anaeromassilibacillus senegalensis* gen. nov., sp. nov., isolated from the gut of a child with kwashiorkor. New Microbes New Infect. 12, 59–60.

Hashimoto K., 2019. Rapid-acting antidepressant ketamine, its metabolites and other candidates: A historical overview and future perspective. Psychiatry Clin. Neurosci. 73, 613–627.

Hashimoto K., 2020. Molecular mechanisms of the rapid-acting and long-lasting antidepressant actions of (*R*)-ketamine. Biochem. Pharmacol. 177, 113935.

Hashimoto, K., 2022. Ketamine: anesthetic, psychotomimetic, antidepressant, or anthelmintic? Mol. Psychiatry 27(8), 3116–3118. doi: 10.1038/s41380-022-01587-7.

Haxaire, C., Hakobyan, N., Pannellini, T., Carballo, C., McIlwain, D., Mak, T.W., Rodeo, S., Acharya, S., Li, D., Szymonifka, J., Song, X., Monette, S., Srivastava, A., Salmon, J.E., Blobel, C.P., 2018. Blood-induced bone loss in murine hemophilic arthropathy is prevented by blocking the iRhom2/ADAM17/TNF-α pathway. Blood 132, 1064–1074.

Hernandez, C.J., Moeller, A.H., 2022. The microbiome: A heritable contributor to bone morphology? Semin. Cell Dev. Biol. 123, 82–87.

Hlis, R.D., McIntyre, R.S., Maalouf, N.M., Enkevort, E.V., Brown, E.S., 2018. Association between bone mineral density and depressive symptoms in a Population-based sample. J. Clin. Psychiatry 79, 16m11276.

Kindilien, S., Goldberg, E.M., Roberts, M.H., Gonzales-Pacheco, D., 2018. Nutrition status, bone mass density, and selective serotonin reuptake inhibitors. Prev. Med.113, 62–67.

Krautkramer, K.A., Fan, J., Bäckhed, F., 2021. Gut microbial metabolites as multi-kingdom intermediates. Nat. Rev. Microbiol. 19(2), 77–94. doi: 10.1038/s41579-020-0438-4.

Levelle, A., Sokol, H., 2020. Gut microbiota-derived metabolites as key actions in inflammatory bowel disease. Nat. Rev. Gastroenterol. Hepatol. 17(4), 223–237.

Leal, G.C., Bandeira, I.D., Correia-Melo, F.S., Telles, M., Mello, R.P., Vieira, F., et al., 2021. Intravenous arketamine for treatment-resistant depression: open-label pilot study. Eur. Arch. Psychiatry Clin. Neurosci. 271(3), 577–582.

Li, K., Zhang, L., Xue, J., Yang, X., Dong, X., Sha, L., Lei, H., Zhang, X., Zhu, L., Wang, Z., Li, X., Wang, H., Liu, P., Dong, Y., He, L., 2019. Dietary inulin alleviates diverse stages of type 2 diabetes mellitus via anti-inflammation and modulating gut microbiota in db/db mice. Food Funct. 10, 1915–1927.

Liu, X.Q., Zhuang, M., Wang, Z., Huber, R.M., 2014. Correlation between dihydropyrimidine dehydrogenase and efficacy and toxicity of fluoropyrimidine drugs. Eur. Rev. Med. Pharmacol. Sci. 18, 2772–2776.

Lu, L., Chen, X., Liu, Y., Yu, X., 2021. Gut microbiota and bone metabolism. FASEB J. 35, e21740.

Parks, D.H., Tyson, G.W., Hugenholtz, P., Beiko, R.G., 2014. STAMP: statistical analysis of taxonomic and functional profiles. Bioinformatics 30, 3123–3124.

Qu, Y., Yang, C., Ren, Q., Ma, M., Dong, C., Hashimoto, K., 2017. Comparison of (*R*)-ketamine and lanicemine on depression-like phenotype and abnormal composition of gut microbiota in a social defeat stress model. Sci. Rep. 7, 15725.

Rizzoli, R., Cooper, C., Reginster, J.Y., Abrahamsen, B., Adachi, J.D., Brandi, M.L., Bruyère, O., Compston, J., Ducy, P., Ferrari, S., Harvey, N.C., Kanis, J.A., Karsenty, G., Laslop, A., Rabenda, V., Vestergaard, P., 2012. Antidepressant medications and osteoporosis. Bone, 51, 606–613.

Rooks, M.G., Garrett, W.S., 2016. Gut microbiota, metabolites and host immunity. Nat. Rev. Immunol. 16(6), 341–352. doi: 10.1038/nri.2016.42.

Sauer, A.K., Grabrucker, A.M., 2019. Zinc deficiency during pregnancy leads to altered microbiome and elevated inflammatory markers in mice. Front. Neurosci. 13, 1295.

Schweiger, J.U., Schweiger, U., Hüppe, M., Kahl, K.G., Greggersen, W., Fassbinder, E., 2016. Bone density and depressive disorder: a meta-analysis. Brain Behav. 6, e00489.

Schymanski, E.L., Jeon, J., Gulde, R., Fenner, K., Ruff, M., Singer, H.P., Hollender, J., 2014. Identifying small molecules via high resolution mass spectrometry: communicating confidence. Environ. Sci. Technol. 48, 2097–2098.

Seely, K.D., Kotelko, C.A., Douglas, H., Bealer, B., Brooks, A.E., 2021. The human gut microbiota: A key mediator of osteoporosis and osteogenesis. Int. J. Mol. Sci. 22, 9452.

Segata, N., Izard, J., Waldron, L., Gevers, D., Miropolsky, L., Garrett, W.S., Huttenhower, C., 2011. Metagenomic biomarker discovery and explanation. Genome Biol. 12(6), R60.

Stubbs, B., Brefka, S., Dallmeier, D., Stubbs, J., Vancampfort, D., Denkinger, M.D., 2016. Depression and reduced bone mineral density at the hip and lumbar spine: a comparative meta-analysis of studies in adults 60 years and older. Psychosom. Med. 78(4), 492–500.

Tsugawa, H., Cajka, T., Kind, T., Ma, Y., Higgins, B., Ikeda, K., Kanazawa, M., VanderGheynst, J., Fiehn, O., Arita, M., 2015. MS-DIAL: data-independent MS/MS deconvolution for comprehensive metabolome analysis. Nat. Methods 12, 523–526.

Tu, Y., Yang, R., Xu, X., Zhou, X., 2021. The microbiota-gut-bone axis and bone health. J. Leukoc. Biol. 110, 525–537.

Wadhwa, R., Kumar, M., Talegaonkar, S., Vohora, D., 2017. Serotonin reuptake inhibitors and bone health: A review of clinical studies and plausible mechanisms. Osteoporos. Sarcopenia 3, 75–81.

Wang, T.J., Larson, M.G., Vasan, R.S., Cheng, S., Rhee, E.P., McCabe, E., Lewis, G.D., Fox, C.S., Jacques, P.F., Fernandez, C., O'Donnell, C.J., Carr, S. A., Mootha, V.K., Florez, J.C., Souza, A., Melander, O., Clish, C.B., Gerszten, R.E., 2011. Metabolite profiles and the risk of developing diabetes. Nat. Med. 17, 448–453.

Wei, Y., Chang, L., Hashimoto, K., 2022a. Molecular mechanisms underlying the antidepressant actions of arketamine: beyond the NMDA receptor. Mol. Psychiatry 27, 559–573.

Wu, Q., Magnus, J.H., Liu, J., Bencaz, A.F., Hentz, J.G., 2009. Depression and low bone mineral density: a meta-analysis of epidemiologic studies. Osteoporos. Int. 20, 1309–1320.

Xiong, Z., Fujita, Y., Zhang, K., Pu, Y., Chang, L., Ma, M., Chen, J., Hashimoto, K., 2019. Beneficial effects of (*R*)-ketamine, but not its metabolite (2*R*,6*R*)-hydroxynorketamine, in the depression-like phenotype, inflammatory bone markers, and bone mineral density in a chronic social defeat stress model. Behav. Brain Res. 368, 111904.

Yang, T.L., Shen, H., Liu, A., Dong, S.S., Zhang, L., Deng, F.Y., Zhao, Q., Deng, H.W., 2020. A road map for understanding molecular and genetic determinants of osteoporosis. Nat. Rev. Endocrinol. 16, 91–103.

Yirmiya, R., Bab, I., 2009. Major depression is a risk factor for low bone mineral density: a meta-analysis. Biol. Psychiatry 66, 423–432.

Zackular, J.P., Baxter, N.T., Iverson, K.D., Sadler, W.D., Petrosino, J.F., Chen, G.Y., Schloss, P.D., 2013. The gut microbiome modulates colon tumorigenesis. mBio 4, e00692-13.

Zhang, J.C., Li, S.X., Hashimoto, K., 2014. *R* (-)-ketamine shows greater potency and longer lasting antidepressant effects than *S* (+)-ketamine. Pharmacol. Biochem. Behav. 116, 137–141.

Zhang, L., Zhan, H., Xu, W., Yan, S., Ng, S.C., 2021. The role of gut mycobiome in health and diseases. Therap. Adv. Gastroenterol. 14, 17562848211047130.

Zhong, X., Zhang, F., Yin, X., Cao, H., Wang, X., Liu, D., Chen, J., Chen, X., 2021. Bone homeostasis and gut microbial-dependent signaling pathways. J. Microbiol. Biotechnol. 31, 765–774.

Neuropharmacology　vol. 213　No. 109139

2022 年 5 月 17 日　公表済

DOI: 10.1016/j.neuropharm.2022.109139

Neuropharmacology　vol. 228　No. 109466

2023 年 2 月 16 日　公表済

DOI: 10.1016/j.neuropharm.2023.109466